Document Number: SET 2015-0010
412 TW-PA-14156

Equalization in Aeronautical Telemetry Using Multiple Antennas

April 2014

Tom Young
SET Executing Agent
412 TENG/ENI
(661) 277-1071
Email: tommy.young.1@us.af.mil

Test Resource Management Center (TRMC)
Test & Evaluation/ Science & Technology (T&E/S&T)
Spectrum Efficient Technology (SET)

REPORT DOCUMENTATION PAGE

Form Approved
OMB No. 0704-0188

1. REPORT DATE *(DD-MM-YYYY)*	**2. REPORT TYPE**	**3. DATES COVERED** *(From - To)*
23-02-2015	Technical Paper/ Journal	3/13 -- 6/15

4. TITLE AND SUBTITLE
Equalization in Aeronautical Telemetry Using Multiple Antennas

5a. CONTRACT NUMBER: W900KK-13-C-0026

5b. GRANT NUMBER: N/A

5c. PROGRAM ELEMENT NUMBER

6. AUTHOR(S)
Michael Rice, Md.; Shah Afran; Mohammad Saquib

5d. PROJECT NUMBER

5e. TASK NUMBER

5f. WORK UNIT NUMBER

7. PERFORMING ORGANIZATION NAME(S) AND ADDRESS(ES)

Brigham Young University, Department of Electrical & Computer Engineering,
459 Clyde Building, Brigham Young University, Provo, UT 84602

8. PERFORMING ORGANIZATION REPORT NUMBER
412TW-PA-14156

9. SPONSORING / MONITORING AGENCY NAME(S) AND ADDRESS(ES)
Test Resource Management Center
Test and Evaluation/ Science and Technology
4800 Mark Center Drive, Suite 07J22
Alexandria, VA 22350

10. SPONSOR/MONITOR'S ACRONYM(S)
N/A

11. SPONSOR/MONITOR'S REPORT NUMBER(S) SET 2015-0010

12. DISTRIBUTION / AVAILABILITY STATEMENT
Approved for public release A: distribution is unlimited.

13. SUPPLEMENTARY NOTES
CA: Air Force Flight Test Center Edwards AFB CA CC: 012100

14. ABSTRACT
This paper introduces a generalized time-reversed space-time block codes (GTR-TRSTBC) as both a conceptual tool to examine the impact of unequal power allocation in equalized single-carrier systems employing two transmit antennas and as a method for exploiting partial channel state information by the transmitter. The generalization involves unequal power allocation parameterized by ρ. The criteria for selecting the optimum ρ is minimizing the residual mean-squared error at the MMSE equalizer output. GTR-STBC is applied to measured channel impulse responses and a simple statistical channel model. The results show that 1) the optimum value of ρ gives the best tradeoff between signal-to-noise ratio and ISI; 2) equal power allocation may not be the optimum power allocation when channel state information is available; and 3) the optimum profile of ρ over measured channels is significantly different than from that in statistical channel models.

15. SUBJECT TERMS
Spectrum, Aeronautical telemetry, algorithm, bandwidth, time-reversed space-time block codes (GTR-TRSTBC)

16. SECURITY CLASSIFICATION OF:			**17. LIMITATION OF ABSTRACT**	**18. NUMBER OF PAGES**	**19a. NAME OF RESPONSIBLE PERSON**
Unclassified					412 TENG/EN (Tech Pubs)
a. REPORT	**b. ABSTRACT**	**c. THIS PAGE**			**19b. TELEPHONE NUMBER** *(include area code)*
Unclassified	Unclassified	Unclassified	None	42	661-277-8615

Standard Form 298 (Rev. 8-98)
Prescribed by ANSI Std. Z39.18

Equalization in Aeronautical Telemetry Using Multiple Antennas

Michael Rice, Md. Shah Afran, Mohammad Saquib

Abstract

This paper introduces a generalized time-reversed space-time block codes (GTR-TRSTBC) as both a conceptual tool to examine the impact of unequal power allocation in equalized single-carrier systems employing two transmit antennas and as a method for exploiting partial channel state information by the transmitter. The generalization involves unequal power allocation parameterized by ρ. The criteria for selecting the optimum ρ is minimizing the residual mean-squared error at the MMSE equalizer output. GTR-STBC is applied to measured channel impulse responses and a simple statistical channel model. The results show that 1) the optimum value of ρ gives the best tradeoff between signal-to-noise ratio and ISI; 2) equal power allocation may not be the optimum power allocation when channel state information is available; and 3) the optimum profile of ρ over measured channels is significantly different than from that in statistical channel models.

I. Introduction

Aeronautical telemetry is a wideband air-to-ground communication link with severe size, weight and power limitations imposed on the airborne transmitter combined with frequency selective fading channels. The size, weight, and power constraints on the airborne platform impose limitations on the transmitter. Many of these needs are met by using highly power-efficient transmitters, such as radio frequency (RF) power amplifiers operating in full saturation. Consequently, given constant-envelope modulations are preferred. This preference manifests itself by the modulations described in the aeronautical telemetry standard IRIG 106 [1]: pulse code modulation with frequency modulation (PCM/FM), shaped offset quaternary phase shift keying

M. Rice is with the Department of Electrical & Computer Engineering, 459 Clyde Building, Brigham Young University, Provo UT 84602. Email: mdr@byu.edu

Md. S. Afran and M. Saquib are with the Department of Electrical Engineering, The University of Texas at Dallas, 800 W. Campbell Road, Richardson, Texas 75080-3021. Emails: mxa121331@utdallas.edu, saquib@utdallas.edu

This work was funded by the Test Resource Management Center (TRMC) Test and Evaluation Science and Technology (T&E/S&T) Program through the U.S. Army Program Executive Office for Simulation, Training and Instrumentation (PEO STRI) under contracts W900KK-09-C-0016 (M4A) and W900KK-13-C-0026 (PAQ).

version TG (SOQPSK-TG) and a version of non-binary, multi-index continuous phase modulation (CPM) called ARTM CPM. PCM/FM is the legacy modulation which, relative to the other two, is not as bandwidth efficient. The importance of SOQPSK-TG has increased over the past 15 years as the availability of bandwidth has come to dominate scheduling and regulatory discussions.

Multipath fading tends to be the dominate impairment in maintaining link availability. Given the high data rates required by modern test articles, the corresponding RF bandwidth of the telemetry signal is such that essentially all multipath fading is frequency selective. Because frequency selective fading leads to inter-symbol interference (ISI), techniques for mitigating ISI using the IRIG 106 modulations (SOQPSK-TG in particular) are of immediate interest.

The goal therefor is one involving single-carrier, constant-envelope modulation operating in a frequency selective channel. This is clearly an equalization and/or diversity problem. Diversity reception, especially by widely separated antennas, is an obvious solution. But given the expense of ground-based receiving installations, this solution has been relatively unpopular at the major test range facilities. On the other hand, transmit diversity can be a workable solution when size, weight, and power constraints allow it. The most common scenario will be one involving multiple transmit antennas with a single receive antenna.

It is well known that multiple antenna systems are capable of increasing reliability or throughput in multipath fading channels. In flat fading, the optimum signaling approach depends on what the transmitter knows [2]. If the transmitter knows the channels between each transmit and receive antenna, then spatio-temporal coding [3] is optimum in that it maximizes signal-to-noise ratio [2]. If the transmitter does not have this knowledge, then a diversity-maximizing orthogonal design (such as the Alamouti code [4]) is optimum [2]. In frequency selective fading, the general approach is to use OFDM and apply these techniques on a per subcarrier basis. Given the constraints described above, OFDM is not a viable approach and approaches suitable to single-carrier modulation are of interest.

In the case of multi-transmit-antenna systems employing single-carrier modulation and operating on frequency selective channels, time-reversed space-time block codes (TR-STBCs) [5]–[9] play the role that the Alamouti code does in frequency non-selective fading with an uninformed transmitter. When the transmitter knows the channels, the situation becomes less clear. Given the fact that SOQPSK-TG does not have any “variable parameters” such as number and location of constellation points, just how an informed transmitter is to use channel state information is not obvious. The only other variable available to the system is the power allocated to each transmit antenna.

In an effort to explore the possibility of transmit diversity to increase the robustness of aeronautical telemetry links prone to multipath fading, channel sounding experiments involving

multiple transmit antennas have been conducted at Cairns Army Airfield, Ft. Rucker, Alabama, [10], [11] and Edwards Air Force Base, California, [20]. Initial experiments involving TR-STBC applied to the channel the helicopter-to-ground channel sets revealed some curious behavior This behavior with TR-STBC, QPSK, and the channel sets was described in [11]. This same behavior TR-STBC, SOQPSK-TG for the same data set is illustrated in Fig. 1. This plot compares the simulated bit error rate (BER) performance of TR-STBC using MMSE equalizers (described in Section III) to the simulated BER performance of a link using only *one* of the two available channels. TR-STBC performs better than the single-channel link using only channel 2, but *worse* than the single-channel link using only channel 1. Clearly, channel 1 is better, in some sense, than channel 2. In fact, channel 1 is so much better than channel 2 that incorporating channel 2 into a TR-STBC system only makes things worse.

In other words, there are cases where it is better to abandon traditional TR-STBC and use only one of the two available channels. The fact that this curious behavior *can* occur on real channels prompts one to ask, "Can this curious behavior be derived from the given impulse responses of two channels?" In other words, it appears that with some form of channel state information, it is possible to achieve better performance than TR-STBC.

This paper answers the question. As a conceptual tool, we consider a fixed-power transmitter that allocates a portion of the fixed power to each channel. This power allocation is parameterized by ρ, the proportion of total power allocated to channel 1. Using only one of the two available channels is captured by the case $\rho = 1$ (channel 1 only) or $\rho = 0$ (channel 2 only). Next, we introduce Generalized TR-STBC (GTR-STBC), a modified version of TR-STBC that incorporates the unequal power allocation ρ. Because TR-STBC and its generalized version involve the combination of diversity processing and equalization, a suitable equalization technique for SOQPSK-TG is needed. We develop and analyze an minimum mean-squared error (MMSE) equalizer that operates on the samples of SOQPSK-TG. Equipped with GTR-STBC and a suitable equalization technique, we use the mean-squared error criterion to identify the optimum ρ. The motivations for the mean-squared error criterion are the following:

1) Mathematically tractable expressions for the mean-squared error at the equalizer output are easily derived [see (42) below].
2) The mean-square error criterion neatly captures the contributions of both ISI and additive noise at the equalizer output.
3) Generally speaking, reductions in mean-squared error lead to reductions in bit error rate.

By expressing the residual mean-squared error at the equalizer output as a function of ρ, we are able to chose ρ to minimize the residual mean-squared error for a given pair of channel impulse responses.

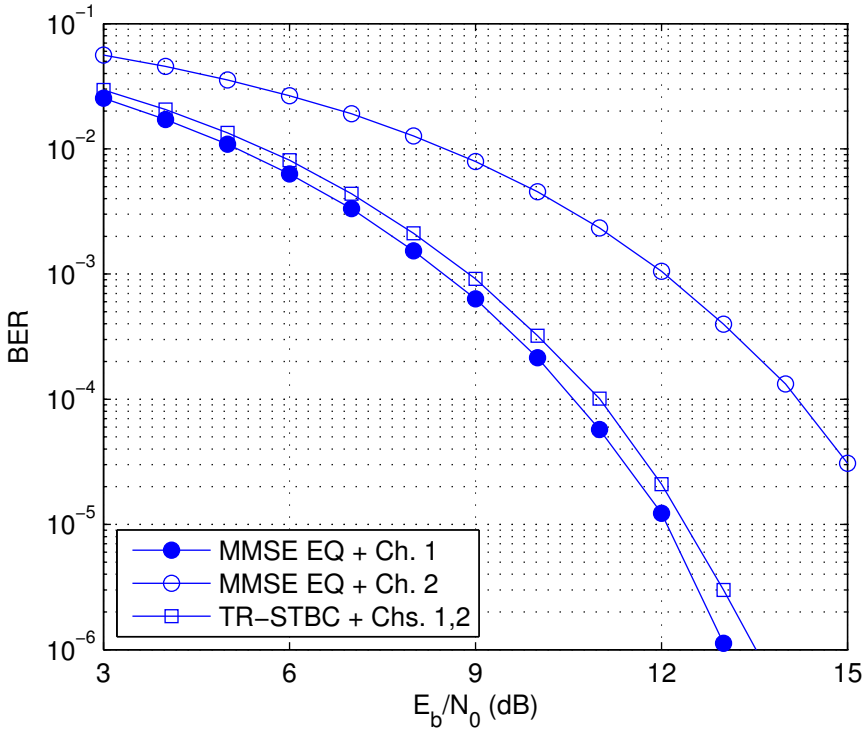

Fig. 1. Simulated BER plots for 10-Mbit/s SOQPSK-TG using MMSE equalizers over a pair of representative impulse responses measured over a helicopter-to-ground channel. The circular markers are the BER results using a single antenna, the square markers are the BER results using both channels with TR-STBC.

Finally, we apply the concepts to the set of measured channel impulse responses to see if the mean-squared error criterion is capable of identifying the cases where the curious behavior occurs. The results show that the mean-squared error criterion does indeed capture the curious behavior.

The conceptual tool of unequal power allocation together with GTR-STBC define a simple transmit diversity scheme based on the partial knowledge of the channel by the transmitter. Here, the transmitter only needs to know ρ, which is easy to compute at the receiver and send back to the transmitter. This simple scheme includes transmit selection diversity ($\rho = 0$ or 1) and traditional TR-STBC ($\rho = 1/2$).

This paper is organized as follows. SOQPSK-TG is described in Section II and the MMSE equalizer for SOQPSK-TG is developed in Section III. GTR-STBC is introduced and analyzed in Section IV. GTR-STBC is applied to the measured channel impulse responses in Section V, and conclusions are presented in Section VI.

II. SOQPSK-TG

Shaped offset QPSK, version TG (SOQPSK-TG) is constant-envelope modulation with good spectral containment and good detection efficiency. For these reasons, it is an ideal choice for aeronautical telemetry and has been a part of the IRIG-106 standard since 2004 [1]. SOQPSK-TG is a continuous phase modulation (CPM) whose complex-valued baseband equivalent representation [12] is

$$x(t, \boldsymbol{\alpha}) = \sqrt{\frac{2E_b}{T_b}} \exp\left[j\left(\phi(t, \boldsymbol{\alpha}) + \phi_0\right)\right]. \tag{1}$$

The phase is

$$\begin{aligned}\phi(t, \boldsymbol{\alpha}) &= 2\pi h \int_{-\infty}^{t} \sum_{n=-\infty}^{\infty} \alpha_n f(\tau - nT_b) d\tau \\ &= 2\pi h \sum_{n=-\infty}^{\infty} \alpha_n q(t - nT_b).\end{aligned} \tag{2}$$

where $f(t)$ is the frequency pulse; $q(t) = \int_{-\infty}^{t} f(\tau) d\tau$ is the phase pulse; ϕ_0 is an arbitrary phase which, without loss of generality, can be set to 0; T_b is the bit interval (or reciprocal of the bit rate); $h = 1/2$ is the modulation index; and $\alpha_n \in \{-1, 0, 1\}$ are the ternary symbols which are related to the binary input symbols $a_n \in \{-1, 1\}$ by [13]

$$\alpha_n = (-1)^{n+1} \frac{a_{n-1}\left(a_n - a_{n-2}\right)}{2}. \tag{3}$$

The frequency pulse for SOQPSK-TG is described in[1] [15], [16]. Because the frequency pulse spans 8 bit times, SOQPSK-TG is a partial response CPM. Consequently, the maximum likelihood detector in the additive white Gaussian noise (AWGN) environment is a sequence estimator [17], usually implemented using the Viterbi algorithm involving a trellis with 512 states. A reduced-complexity, near optimum 4-state detector was described in [15]. The most common detector applied to SOQPSK-TG is the simple OQPSK-type symbol-by-symbol (SxS) detector described by Perrins [18]. The SxS detector comprises a detection filter (see Fig. 3 of [18]) whose output is sampled at 1 sample/bit and is treated as offset QPSK.

III. MMSE Equalization of SOQPSK-TG

The system considered here is summarized in Figure 2. As before, the complex-valued baseband equivalent representation [12] is used for all signals. Starting with the block diagram of

[1]The basic form was first introduced by Hill in [14] where "-A" and "-B" versions were described. SOQPSK-A has a slightly narrower bandwidth (measured at the -60 dB level) and slightly worse detection efficiency than SOQPSK-B. The Telemetry Group (TG) of the Range Commanders Council adopted the compromise waveform, designated SOQPSK-TG in 2004.

Figure 2 (a), the SOQPSK-TG signal $x_c(t)$ is transmitted through a channel impulse response $h_c(t)$ whose output, accompanied by thermal noise, forms the receive signal $r_c(t)$. After the application of an anti-aliasing low-pass filter with impulse response $h_a(t)$, T-spaced samples of $r_c(t)$ are produced by an A/D converter. Assuming the anti-aliasing filter does not distort the received signal, the samples of the received signal may be expressed as

$$r(n) = x(n) * h(n) + w(n) = \sum_{k=-L_1}^{L_2} h(k)x(n-k) + w(n) \tag{4}$$

where

$$r(n) = r_c(nT) \qquad x(n) = x_c(nT) \qquad h(n) = h_c(t) * h_a(t)|_{t=nT}$$

and where the $w(n)$ is the n-th sample in a sequence zero-mean complex-valued Gaussian random variables with autocorrelation function

$$R_w(k) = \frac{1}{2}\mathrm{E}\left\{w(n)w^*(n-k)\right\} = \sigma_w^2\delta(k). \tag{5}$$

Note that (4) assumes the discrete-time channel has support on $-L_1 \leq n \leq L_2$. As a first step, we apply the samples $r(n)$ to a filter matched to the disccrete-time channel to produce $y(n)$:

$$\begin{aligned} y(n) &= r(n) * h^*(-n) \\ &= x(n) * \underbrace{h(n) * h^*(-n)}_{h_{\text{eq}}(n)} + \underbrace{w(n) * h^*(-n)}_{v(n)} \qquad (6) \\ &= \sum_{k=-L_{\text{eq}}}^{L_{\text{eq}}} h_{\text{eq}}(k)x(n-k) + v(n) \qquad (7) \end{aligned}$$

where $L_{\text{eq}} = L_1 + L_2$ and $v(n)$ is a complex valued Gaussian random sequence with zero mean and autocorrelation function

$$R_v(k) = \frac{1}{2}\mathrm{E}\left\{v(n)v^*(n-k)\right\} = \sigma_w^2 h_{\text{eq}}(k). \tag{8}$$

The samples $y(n)$ form the input to an MMSE equalizer. The MMSE equalizer is an FIR filter with coefficients $c(n)$ for $-L_c \leq n \leq L_c$ designed to minimize the mean squared error between the equalizer filter output $\hat{x}(n)$ and the sequence $x(n)$. The entire system may be represented by an equivalent discrete-time system shown in Figure 2 (b).

The challenge with equalizing *samples* of the modulated signal is that the underlying continuous-time waveform is not wide-sense stationary [12]. This fact carries over to the samples of $x_c(t)$

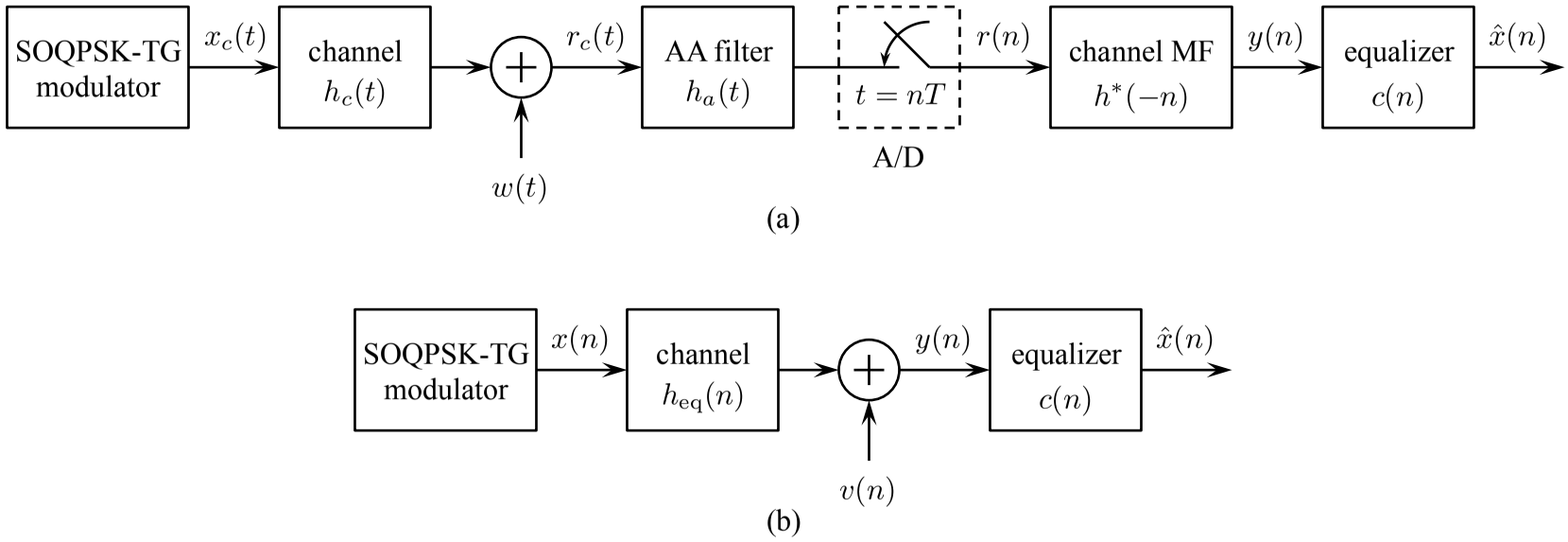

Fig. 2. A block diagram of the system that applies an MMSE equalizer to samples of a received SOQPSK-TG signal: (a) the system showing the continuous-time signals, the anti-aliasing filter, and A/D converter; (b) the equivalent discrete-time system.

and is captured by the fact that the autocorrelation function of the $x(n)$ is of the form

$$R_x(k,\ell) = \frac{1}{2}\mathrm{E}\left\{x(k)x^*(\ell)\right\}, \tag{9}$$

that is, the autocorrelation function is a function of both sample indexes, not the difference between them. Consequently, the equalizer filter coefficients are a function of the sample index n. It is hard to see how this solution has any practical utility, especially in the presence of a real-time performance requirement. In the end, the designer is left with suboptimal approaches of reduced computational complexity whose accompanying performance penalty is acceptable.

The simplest suboptimal approach is to assume the signal samples are wide-sense stationary. Here, the autocorrelation function is of the form

$$R_x(k-\ell) = \frac{1}{2}\mathrm{E}\left\{x(k)x^*(\ell)\right\}, \tag{10}$$

that is, the autocorrelation function depends on the difference of the sample time indexes. The wide-sense stationary assumption for $x(n)$ greatly simplifies the solution. Because the optimum equalizer coefficients no longer depend on the samples index n, the relationship between $x(n)$ and the equalizer output $\hat{x}(n)$ is

$$\hat{x}(n) = c(n) * y(n) = \sum_{k=-L_c}^{L_c} c(k)y(n-k). \tag{11}$$

The vector of filter coefficients that minimizes the mean squared error

$$\mathcal{E} = \mathrm{E}\left\{\left|x(n) - \hat{x}(n)\right|^2\right\} \tag{12}$$

is given by

$$\mathbf{c} = \left[\mathbf{G}\mathbf{R}_{x,1}\mathbf{G}^\dagger + \mathbf{R}_v\right]^{-1}\mathbf{R}_{x,2}\mathbf{g}^\dagger \tag{13}$$

where $\mathbf{c}$ is the $(2L_c+1)\times 1$ vector of filter coefficients, $\mathbf{G}$ is the $(2L_c+1)\times(2L_c+1+2L_{\text{eq}})$ matrix

$$\mathbf{G} = \begin{bmatrix} h_{\text{eq}}(L_c) & \cdots & h_{\text{eq}}(-L_c) & & \\ & h_{\text{eq}}(L_c) & \cdots & h_{\text{eq}}(-L_c) & \\ & & \ddots & & \\ & & & h_{\text{eq}}(L_c) & \cdots \quad h_{\text{eq}}(-L_c) \end{bmatrix}; \tag{14}$$

$\mathbf{R}_{x,1}$ is the $(2L_c + 2L_{\text{eq}} + 1) \times (2L_c + 2L_{\text{eq}} + 1)$ matrix

$$\mathbf{R}_{x,1} = \begin{bmatrix} R_x(0) & R_x(-1) & \cdots & R_x(-2L_c - 2L_{\text{eq}}) \\ R_x(1) & R_x(0) & \cdots & R_x(-2L_c - 2L_{\text{eq}} + 1) \\ \vdots & & & \vdots \\ R_x(2L_c + 2L_{\text{eq}}) & R_x(2L_c + 2L_{\text{eq}} - 1) & \cdots & R_x(0) \end{bmatrix}; \tag{15}$$

$\mathbf{R}_v$ is the $(2L_c + 1) \times (2L_c + 1)$ noise autocorrelation matrix given by

$$\mathbf{R}_v = \begin{bmatrix} R_v(0) & \cdots & R_v(-2L_c) \\ \vdots & & \vdots \\ R_v(2L_c) & \cdots & R_v(0) \end{bmatrix}; \tag{16}$$

$\mathbf{R}_{x,2}$ is the $(2L_c + 1) \times (2L_c + 1)$ matrix given by

$$\mathbf{R}_{x,2} = \begin{bmatrix} R_x(0) & R_x(-1) & \cdots & R_x(-2L_c) \\ R_x(1) & R_x(0) & \cdots & R_x(-2L_c + 1) \\ \vdots & & & \vdots \\ R_x(2L_c) & R_x(2L_c + 1) & \cdots & R_x(0) \end{bmatrix}; \tag{17}$$

and $\mathbf{g}$ is the $1 \times (2L_c + 2L_{\text{eq}} + 1)$ vector given by

$$\mathbf{g} = \begin{bmatrix} \mathbf{0}_{1\times(L_c - L_{\text{eq}})} & \mathbf{h}_{\text{eq}} & \mathbf{0}_{1\times(L_c - L_{\text{eq}})} \end{bmatrix} \tag{18}$$

where $\mathbf{0}_{1\times(L_c - L_{\text{eq}})}$ is a row vector comprising $L_c - L_{\text{eq}}$ zeros (here we assume $L_c > L_{\text{eq}}$, i.e., the equalizer is longer than the channel), and $\mathbf{h}_{\text{eq}}$ is the $1 \times (2L_{\text{eq}} + 1)$ vector given by

$$\mathbf{h}_{\text{eq}} = \begin{bmatrix} h_{\text{eq}}(L_{\text{eq}}) & \cdots & h_{\text{eq}}(0) & \cdots & h_{\text{eq}}(-L_{\text{eq}}) \end{bmatrix}. \tag{19}$$

The question is now, what function should be used for the autocorrelation function $R_x(k)$? Two approximations are investigated here. The first is an empirically-derived autocorrelation function. The empirical autocorrelation function is obtained by generating a large number of samples $x(n)$ and using the standard estimation technique assuming wide sense stationarity. Given L samples of $x(n)$ for $n = 0, 1, \ldots, L-1$, this empirical autocorrelation function is

$$R_{\text{e}}(k) = \frac{1}{2(L-k)} \sum_{n=k}^{L-1} x(n)x^*(n-k), \qquad 0 \le k < L-1 \tag{20}$$

together with

$$R_{\text{e}}(k) = R_{\text{e}}^*(-k), \qquad -L < k < 0. \tag{21}$$

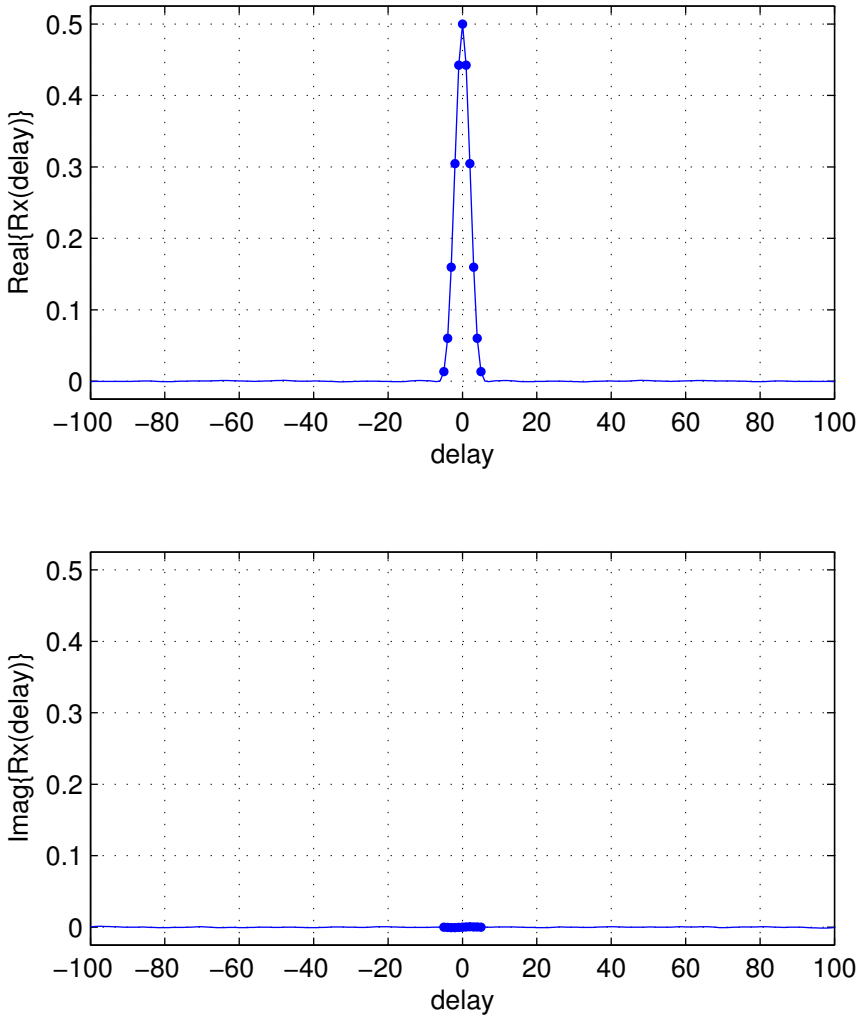

Fig. 3. A plot of the empirical autocorrelation function for SOQPSK-TG: (top) the real part of $R_{\rm e}(k)$; (bottom) the imaginary part of $R_{\rm e}(k)$. The sample rate for the SOQPSK-TG samples is at 2 samples/bit. Markers indicate the values for $-5 \leq k \leq 5$.

A plot of $R_{\rm e}(k)$ corresponding to $L = 2 \times 10^6$ samples of SOQPSK-TG sampled at 2 samples/bit is shown in Figure 3 for the first 100 lags (i.e., $-100 \leq k \leq 100$). The top plot shows the real part of $R_{\rm e}(k)$ and the lower plot shows the imaginary part of $R_{\rm e}(k)$. The only significant values are those for $-5 \leq k \leq 5$ and indicated by markers on the plot. Consequently, in the simulation results presented below, we assume $R_{\rm e}(k) = 0$ for $|k| > 5$.

The second approximation is to assume the data are uncorrelated. This generates a correlation function of the form

$$R_{\rm i}(k) = \sigma_x^2 \delta(k). \tag{22}$$

Here, the corresponding correlation matrices $\mathbf{R}_{x,1}$ and $\mathbf{R}_{x,2}$ are scaled identity matrices and they function as regularizers in the numerical computations (13).

To test the performance of these approximations, we simulate the performance of the equalized SOQPSK-TG system outlined in Figure 4. For this test, we use a channel obtained from our channel measurement campaign described below with $L_{\text{eq}} = 19$ and operating at $N = 2$ samples/bit. The channel transfer function is plotted in Figure 5. The equalizer output is applied to the symbol-by-symbol detector for SOQPSK-TG (denoted "S$\times$S detector" in the figure) described in Section II.

The effectiveness of using $R_{\text{e}}(k)$ and $R_{\text{i}}(k)$ in computing the equalizer coefficients was measured by the simulated bit error rate. The simulations applied the equalizer coefficients obtained from (13) for $L_c = 5 \times L_{\text{eq}} = 95$ [19] and using $R_{\text{e}}(k)$ and $R_{\text{i}}(k)$. The simulated bit error rate is plotted in Figure 6, where we observe that there is essentially no difference in the performance between the two. Consequently, we prefer $R_{\text{i}}(k)$ over $R_{\text{e}}(k)$ in what follows because this choice simplifies the computations of the equalizer filter coefficients. In this case, the optimum equalizer filter coefficients are given by

$$\mathbf{c} = \left[\mathbf{G}\mathbf{G}^{\dagger} + \frac{1}{2(E_b/N_0)}\mathbf{H}_{\text{eq}}\right]^{-1} \mathbf{g}^{\dagger} \tag{23}$$

where $\mathbf{H}_{\text{eq}}$ is the $(2L_c + 1) \times (2L_c + 1)$ matrix given by

$$\mathbf{H}_{\text{eq}} = \begin{bmatrix} h_{\text{eq}}(0) & \cdots & h_{\text{eq}}(-2L_c) \\ \vdots & & \vdots \\ h_{\text{eq}}(2L_c) & \cdots & h_{\text{eq}}(0) \end{bmatrix} \tag{24}$$

where it is understood that $h_{\text{eq}}(k) = 0$ for $|k| > L_{\text{eq}}$. The corresponding mean squared error is

$$\mathcal{E}_{\text{min}} = \sigma_x^2 \left(1 - \mathbf{g}\left[\mathbf{G}\mathbf{G}^{\dagger} + \frac{1}{2(E_b/N_0)}\mathbf{H}_{\text{eq}}\right]^{-1} \mathbf{g}^{\dagger}\right). \tag{25}$$

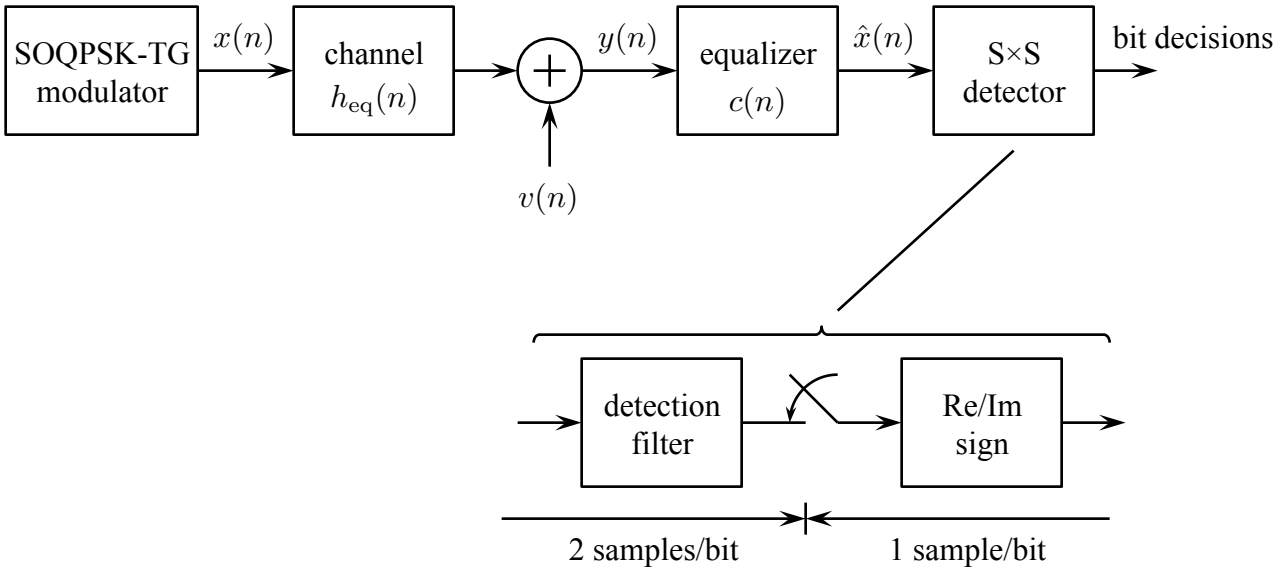

Fig. 4. A block diagram of the system used to test the performance of the SOQPSK-TG autocorrelation assumptions.

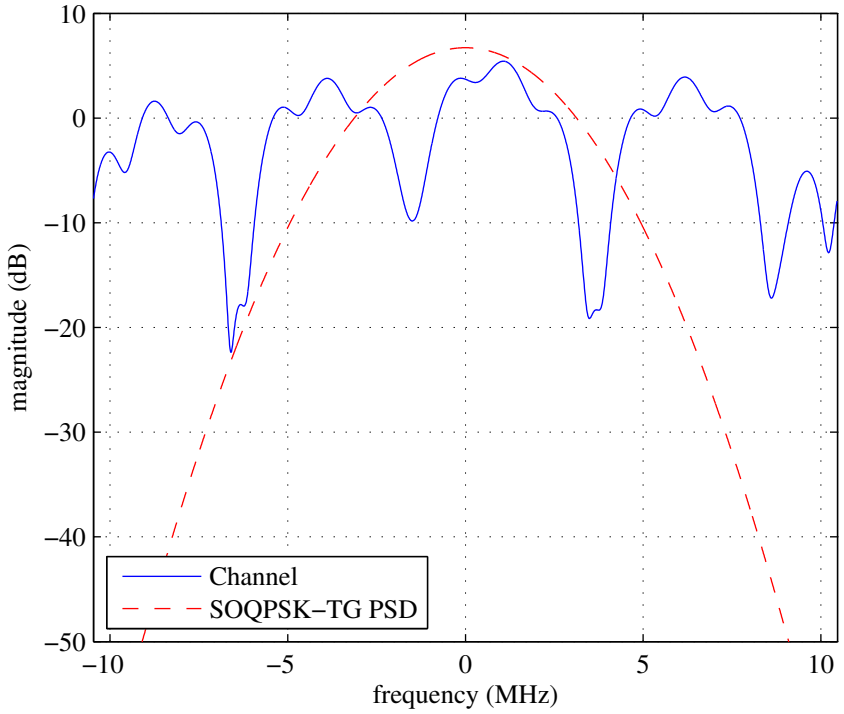

Fig. 5. The channel used in the simulations reported in Figure 6. The channel is obtained from channel measurements described below. The bit rate is 10 Mbits/s and the channel is sampled at 2 samples/bit. The corresponding $h_{\rm eq}(n)$ has $L_{\rm eq} = 19$.

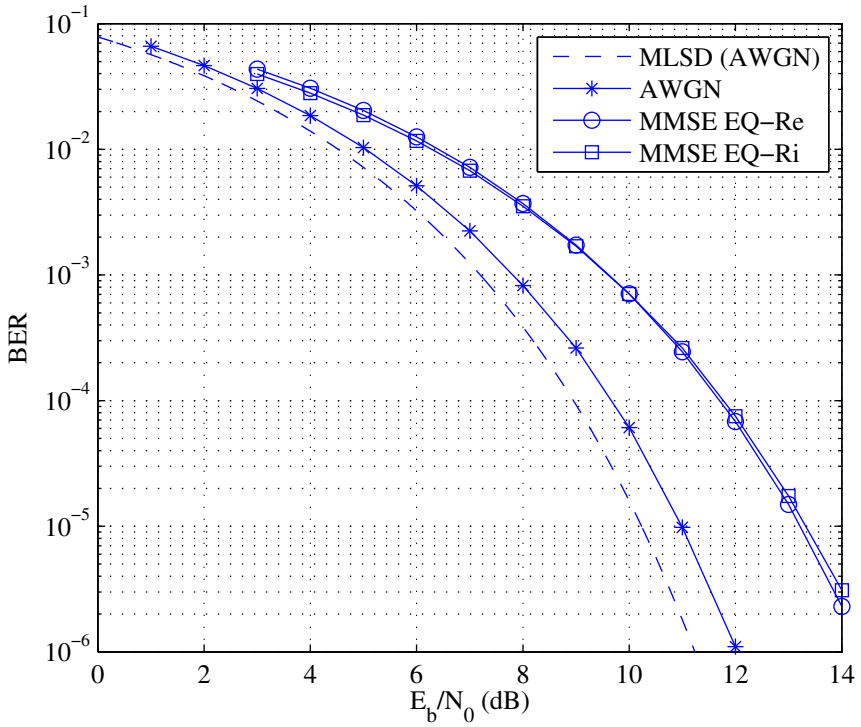

Fig. 6. Simulated bit error rate results for the system shown in Figure 4 using the channel illustrated in Figure 5. Also included for reference is the performance of the symbol-by-symbol detector in the AWGN channel and the optimum maximum likelihood sequence detector (MLSD) in the AWGN channel (see [18]).

IV. Generalized TR-STBC (GTR-STBC): Non-Equal Power Allocations Using TR-STBC

An abstraction (to the sample level) for a 2×1 TR-STBC system is illustrated in Fig. 7. Here the system transmits $2L$ samples of an SOQPSK-TG signal sampled at N samples/bit over two transmit antennas to one receive antenna. The equivalent discrete-time channel between transmit antenna 1 and the receive antenna is represented by the impulse response $h_1(n)$ for $-L_{1,1} \leq n \leq L_{1,2}$ whereas the equivalent discrete-time channel between transmit antenna 2 and the receive antenna is represented by the impulse response $h_2(n)$ for $-L_{2,1} \leq n \leq L_{2,2}$.

The TR-STBC encoder partitions the sample sequence $x(0), \ldots, x(2L-1)$ into two sequences $x_1(n)$ and $x_2(n)$ as shown in Fig. 7. The length-$2L$ packet is transmitted in two intervals[2] each spanning L sample intervals. During the first interval $x_1(0), \ldots, x_1(L-1)$ is transmitted from antenna 1 whereas $x_2(0), \ldots, x_2(L-1)$ is transmitted from antenna 2. During the second interval, $x_2^*(L-1), \ldots, x_2^*(0)$ is transmitted from antenna 1 whereas $-x_1^*(L-1), \ldots, -x_1^*(0)$ is transmitted from antenna 2.

Power division using $0 \leq \rho \leq 1$ is accomplished by modified the TR-STBC system along the lines illustrated in Fig. 7. Amplitude scaling is applied to the signals entering each channel so as to divide the power between the channels. Here ρ represents the proportion of total power allocated to transmit antenna 1. The traditional TR-STBC system[3] is a special case for which $\rho = 1/2$. The square-root is used in Fig. 7 because the amplitudes are what are being modified—the energy (or power) is the square of the amplitude.

The received signal $r(n)$ is given by

$$r(n) = \sqrt{\rho} x_1(n) * h_1(n) + \sqrt{1-\rho} x_2(n) * h_2(n) + w(n) \tag{26}$$

where $w(n)$ is a complex-valued Gaussian random sequence with zero mean and autocovariance function given by (5). The TR-STBC decoder partitions $r(n)$ into $r_1(n)$ and $r_2(n)$ as follows:

$$\begin{aligned} r_1(n) &= r(n) \text{ for } 0 \leq n \leq L-1 \\ r_2(n-L) &= r(n) \text{ for } L \leq n \leq 2L-1. \end{aligned} \tag{27}$$

[2]In a practical implementation, a guard interval at least as long as the longest channel impulse response must be inserted between the two intervals. Here, such an interval is assumed, although we won't complicate the notation to make this explicit.

[3]In the traditional TR-STBC system, $\rho = 1/2$ is included in neither the development nor the notation because the same power is assumed to be applied to each channel. Hence there is no need to account for it, other than in normalizing the noise variance.

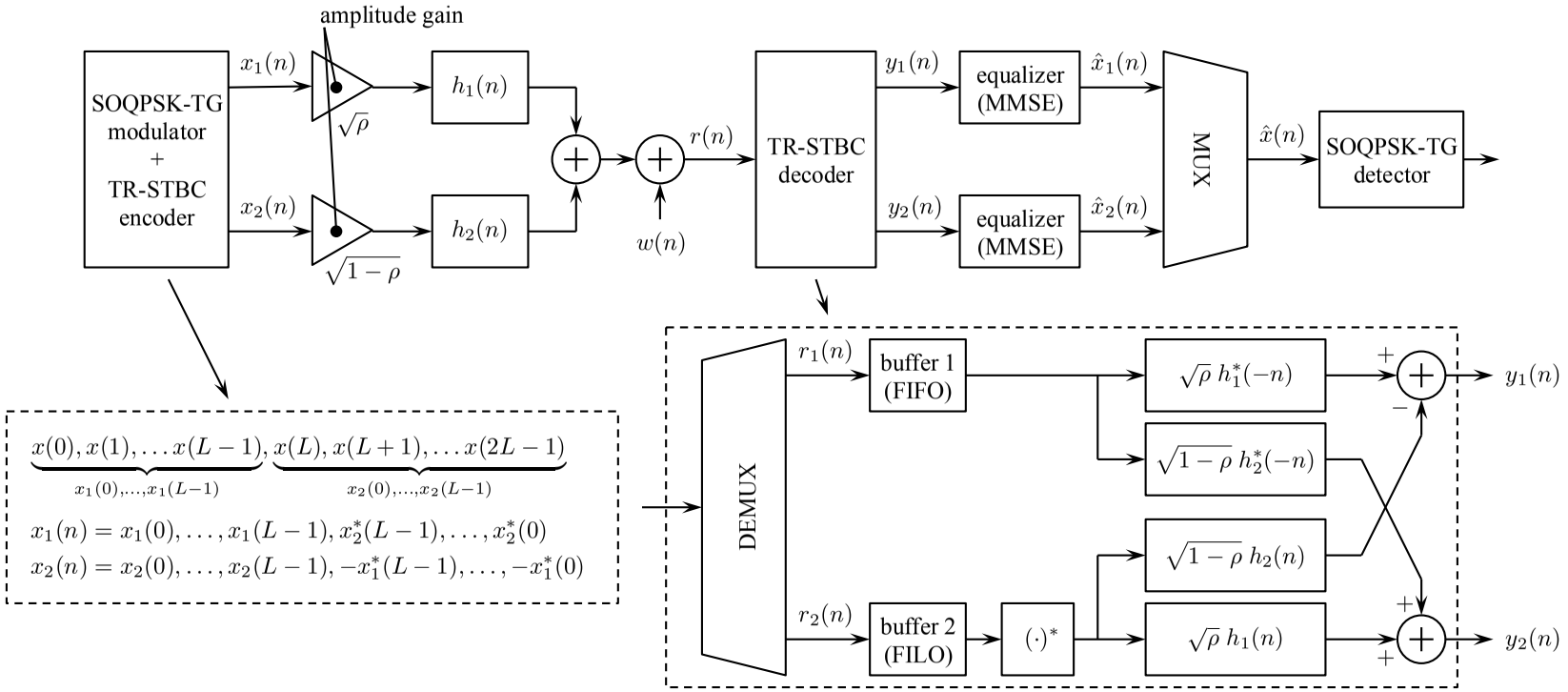

Fig. 7. A block diagram of the TR-STBC system based on unequal power allocation using $0 \leq \rho \leq 1$.

These two sequences are given by

$$r_1(n) = \sqrt{\rho}\, x_1(n) * h_1(n) + \sqrt{1-\rho}\, x_2(n) * h_2(n) + w_1(n) \tag{28}$$

$$r_2(n) = \sqrt{\rho}\, x_2^*(-n) * h_1(n) - \sqrt{1-\rho}\, x_1^*(-n) * h_2(n) + w_2(n) \tag{29}$$

where $w_1(n)$ and $w_2(n)$ are related to $w(n)$ the same way $r_1(n)$ and $r_2(n)$ are related to $r(n)$. The TR-STBC decoder processes $r_1(n)$ and $r_2(n)$ using a bank of filters based on the channel impulse responses $h_1(n)$ and $h_2(n)$ as shown. The result of this processing is a pair of parallel sequences $y_1(n)$ and $y_2(n)$ which may be expressed as

$$\begin{aligned} y_1(n) &= r_1(n) * \sqrt{\rho}\, h_1^*(-n) - r_2^*(-n) * \sqrt{1-\rho}\, h_2(n) \\ &= x_1(n) * \underbrace{\Big[\rho\, h_1(n) * h_1^*(-n) + (1-\rho)\, h_2(n) * h_2^*(-n)\Big]}_{h_{\text{eq}}(n)} \\ &\qquad + \underbrace{w_1(n) * \sqrt{\rho}\, h_1^*(-n) + w_2^*(-n) * \sqrt{1-\rho}\, h_2(n)}_{v_1(n)} \end{aligned} \tag{30}$$

$$\begin{aligned} y_2(n) &= r_1(n) * \sqrt{1-\rho}\, h_2^*(-n) + r_2^*(-n) * \sqrt{\rho}\, h_1(n) \\ &= x_2(n) * \underbrace{\Big[(1-\rho)\, h_2(n) * h_2^*(-n) + \rho\, h_1^*(-n) * h_1(n)\Big]}_{h_{\text{eq}}(n)} \\ &\qquad + \underbrace{\sqrt{1-\rho}\, w_1(n) * h_2^*(-n) + \sqrt{\rho}\, w_2^*(-n) * h_1(n)}_{v_2(n)}. \end{aligned} \tag{31}$$

These equations show that the equivalent composite channel for non-equal power allocation is

$$h_{\text{eq}}(n) = \rho\, \underbrace{h_1(n) * h_1^*(-n)}_{\eta_1(n)} + (1-\rho)\, \underbrace{h_2(n) * h_2^*(-n)}_{\eta_2(n)}. \tag{32}$$

Because the support for $h_1(n)$ is $-L_{1,1} \le n \le L_{1,2}$, the support for $\eta_1(n)$ is $-(L_{1,1}+L_{1,2}) \le n \le (L_{1,1}+L_{1,2})$. Similarly because the support for $h_2(n)$ is $-L_{2,1} \le n \le L_{2,2}$, the support for $\eta_2(n)$ is $-(L_{2,1}+L_{2,2}) \le n \le (L_{2,1}+L_{2,2})$. Consequently, the support for $h_{\text{eq}}(n)$ is $-L_{\text{eq}} \le n \le L_{\text{eq}}$ where

$$L_{\text{eq}} = \max\Big\{L_{1,1}+L_{1,2}, L_{2,1}+L_{2,2}\Big\}. \tag{33}$$

The noise sequences $v_1(n)$ and $v_2(n)$ are complex-valued Gaussian random sequences each with

zero mean and autocorrelation and cross correlation functions

$$\frac{1}{2}\mathrm{E}\left\{v_1(n)v_1^*(n-k)\right\} = \frac{1}{2}\mathrm{E}\left\{v_2(n)v_2^*(n-k)\right\} = \sigma_w^2 h_{\text{eq}}(k). \tag{34}$$

$$\mathrm{E}\left\{v_1(n)v_2^*(n-k)\right\} = 0. \tag{35}$$

By way of summary, the TR-STBC system presents to the equalizers the sequences $y_1(n)$ and $y_2(n)$ which may be represented by

$$y_1(n) = x_1(n) * h_{\text{eq}}(n) + v_1(n) \tag{36}$$

$$y_2(n) = x_2(n) * h_{\text{eq}}(n) + v_2(n) \tag{37}$$

where $h_{\text{eq}}(n)$ is given by (32). The noise terms $v_1(n)$ and $v_2(n)$ are uncorrelated zero-mean Gaussian random sequences each with autocorrelation function (34). A pair of equalizers operate in parallel on $y_1(n)$ and $y_2(n)$. Because the the noise sequences $v_1(n)$ and $v_2(n)$ are statistically equivalent and $h_{\text{eq}}(n)$ is common to both, the pair of equalizers operating on $y_1(n)$ and $y_2(n)$ are identical as long as $a_1(n)$ and $a_2(n)$ are statistically equivalent (the usual case). Any equalizer can be applied here (linear or non-linear, with or without noise whitening) with the usual performance-complexity tradeoffs. Here, we apply the approximate MMSE equalizer introduced in Section III because the MMSE equalizer permit a mathematically tractable analysis for the resulting mean-squared error. We leverage the analytical expression to find the value of ρ that minimizes the mean squared error.

The equalizer filters of Fig. 7 are identical, and the vector of filter coefficients is given by (23) and the corresponding mean squared error is given by (25). In these equations, $\mathbf{G}$, $\mathbf{g}$, and $\mathbf{H}_{\text{eq}}$ may be expressed in terms of power allocation parameter ρ. Using (32), it is straightforward to show that

$$\mathbf{G} = \rho\mathbf{G}_1 + (1-\rho)\mathbf{G}_2 \tag{38}$$

$$\mathbf{g} = \rho\mathbf{g}_1 + (1-\rho)\mathbf{g}_2 \tag{39}$$

$$\mathbf{H}_{\text{eq}} = \rho\mathbf{H}_1 + (1-\rho)\mathbf{H}_2 \tag{40}$$

where $\mathbf{G}_1$, $\mathbf{g}_1$, and $\mathbf{H}_1$ are formed from $\eta_1(n)$ the same way $\mathbf{G}$, $\mathbf{g}$, and $\mathbf{H}_{\text{eq}}$ are formed from $h_{\text{eq}}(n)$, respectively. Similar definitions apply to $\mathbf{G}_2$, $\mathbf{g}_2$, and $\mathbf{H}_2$ with $\eta_2(n)$. Making the substitutions for $\mathbf{G}$, $\mathbf{g}$, and $\mathbf{H}_{\text{eq}}$ gives

$$\mathbf{c} = \mathbf{M}^{-1}\left(\rho\mathbf{g}_1 + (1-\rho)\mathbf{g}_2\right)^{\dagger} \tag{41}$$

and

$$\mathcal{E}_{\min} = \sigma_x^2 \left[1 - \Big(\rho \mathbf{g}_1 + (1-\rho)\mathbf{g}_2 \Big) \, \mathbf{M}^{-1} \, \Big(\rho \mathbf{g}_1 + (1-\rho)\mathbf{g}_2 \Big)^{\dagger} \right] \tag{42}$$

where

$$\mathbf{M} = \Big(\rho \mathbf{G}_1 + (1-\rho)\mathbf{G}_2 \Big) \Big(\rho \mathbf{G}_1 + (1-\rho)\mathbf{G}_2 \Big)^{\dagger} + \frac{1}{2(E_b/N_0)} \Big(\rho \mathbf{H}_1 + (1-\rho)\mathbf{H}_2 \Big) . \tag{43}$$

Equation (42) is the desired relationship: for a given pair of channels $h_1(n)$ and $h_2(n)$, it expresses the mean squared error at the output of the MMSE equalizer as a function of the power allocation ρ. Thus, for a fixed pair channels, one can choose the power allocation to minimize the achievable mean-squared error.

V. Numerical Results

The forgoing analysis was applied to measured impulse responses from four multipath environments typically encountered in aeronautical telemetry. For the modulation, we assume 10 Mbit/s SOQPSK-TG with the equalizers operating at 2 samples/bit. In each of the four cases, we compute the optimum power allocation parameter ρ to a pair of channels labeled $h_1(n)$ and $h_2(n)$. The physical meaning of these channels depends on the scenario as described below.

Two normalizations are applied to the channels: the *natural normalization* and the *equal-energy normalization*. Let $h_{1,\mathrm{u}}(n)$ and $h_{2,\mathrm{u}}(n)$ be unnormalized channel impulse responses for the two equivalent discrete-time channels obtained directly from the channel sounding data, and let

$$E_1 = \sum_{n=-L_{1,1}}^{L_{1,2}} |h_{1,\mathrm{u}}(n)|^2 \qquad E_2 = \sum_{n=-L_{2,1}}^{L_{2,2}} |h_{2,\mathrm{u}}(n)|^2 \tag{44}$$

be the energies in two channels. The natural normalization uses

$$h_1(n) = \frac{1}{\sqrt{E}} h_{1,\mathrm{u}}(n) \qquad h_2(n) = \frac{1}{\sqrt{E}} h_{2,\mathrm{u}}(n) \tag{45}$$

where $E = \max\{E_1, E_2\}$. This normalizes the stronger of the two channels to unit energy.[4] We call this the natural normalization because in real multi-antenna scenarios, it is often the case that one of the channels is stronger than the other.

For the equal-energy normalization, we use

$$h_1(n) = \frac{1}{\sqrt{E_1}} h_{1,\mathrm{u}}(n) \qquad h_2(n) = \frac{1}{\sqrt{E_2}} h_{2,\mathrm{u}}(n). \tag{46}$$

[4]The motivation for unit energy is for scaling the noise variance to define the signal-to-noise ratio.

Here, both channels are normalized to unit energy. This is more typical of statistical or mathematical models of multi-antenna propagation and is a common feature of the more academic approach.

The numerical results were produced as follows. For each pair of channel impulse responses, the impulse responses were normalized using one of the two procedures described above. The value of ρ that minimizes (42) for $L_c = 5 \times L_{\text{eq}}$ [19] was computed.

A. Cairns Army Airfield, Ft. Rucker, Alabama

The first data set comprises channel impulse responses collected at Cairns Army Airfield, Ft. Rucker, Alabama. Here the transmitter was a UH-1H helicopter equipped with 4 transmit antennas as illustrated in Figure 8. The helicopter flight path, the multipath environment, and the locations of the receive antennas are shown in Figure 9. The ground station comprised 6-ft diameter and 4-ft diameter tracking dishes, labeled RX1 and RX2, respectively, located as shown in Figure 8. The channel sounding signal, occupying 50 MHz of bandwidth and centered at 1800 MHz (upper L-band), was used to probe the channel. The resulting impulse responses were resampled to 20 Msamples/s to produce a channel for 10 Mbit/s SOQPSK-TG sampled at 2 samples/bit. Additional details are available in [10].

During the flight line run, the UH-1H maintained an altitude between 15 and 20 ft. AGL. The receive antennas were positioned on 60 ft. towers. The hangers along the flight line are also 60 ft. tall at the roof centers. Consequently, line-of-sight propagation is not possible when a hanger is between the UH-1H and the receive antennas. Consequently this data set represents a rich multipath propagation environment.

To illustrate the behavior of ρ, we assign to $h_1(n)$ the resampled version of $h_{c,2,1}(t)$ [transmission from the nose antenna] and to $h_2(n)$ the resampled version of $h_{c,2,4}(t)$ [transmission from the tail antenna]. The forward-to-aft separation between the two transmit antennas was 400 inches (approximately 61 wavelengths at 1800 MHz). When the UH-1H is level, tail antenna is 43 inches (approximately $6^1/_2$ wavelengths at 1800 MHz) higher than the nose antenna. During flight, the helicopter pitches forward (as suggested in Figure 8) and this places the tail antenna somewhat more than 43 inches higher than the nose antenna.

The locations of the two transmit antennas and the receive antenna produce impulse responses with significant (and similar) degrees of ISI and similar energies, although there will be locations where the propagation path between one of the two transmit antennas and the receiver will be more attenuated than the other and where the ISI on one channel may be much less severe than on the other. Thus, this set of 39,300 impulse response pairs represents a rich mixture of varying signal-to-noise ratios and ISI.

The results using the natural normalization are summarized by the histograms shown in Fig. 10. Curiously, 11,454 of the 39,300 values of ρ for $E_b/N_0 = 10$ dB [Fig. 10 (a)] are close to either 0 or 1. This means approximately 29% of the channel pairs prefer the use of a single channel over the use of both channels. The remaining 27,86 channel pairs minimize the mean squared error by applying some portion of the available transmit power to both antennas. As the signal-to-noise ratio increases to 20 dB [Fig. 10 (b)], the number of occurrences where the single antenna solution is best falls to 5,366 or 14% of the channel pairs. This indicates that as signal-to-noise ratio increases, ISI plays an increasingly dominant role in determining the power allocation that minimizes the mean squared error. The more similar a pair of channels are from the ISI point of view, the more $\rho = 1/2$ minimizes the mean squared error. This suggests that when the signal-to-noise ratio penalty is removed from the weaker of the two channels, an even stronger preference for $\rho = 1/2$ should be observed.

That this is true is documented by the histograms in Figure 11. In Figure 11 (a), 710 of the 39,300 channel pairs (2%) prefer only one of the channels when $E_b/N_0 = 10$ dB and in Figure 11 (b), 743 of the 39,300 channel pairs (2%) prefer only one of the channels when $E_b/N_0 = 20$ dB.

In summary, the results for a multipath-rich environment show that when signal-to-noise ratio is moderate and the channels are not normalized to equal energy, applying 100% of the available power to one of the two transmit antennas, is frequently the solution that minimizes the mean squared error. As signal-to-noise ratio increases, or the signal-to-noise ratio penalty of the weaker channel is removed, applying 100% of the available power to one of the two antennas is less often the solution that minimizes the mean squared error. In this case, as long as the channels have similar degrees of ISI, applying power to both channels becomes the best thing to do.

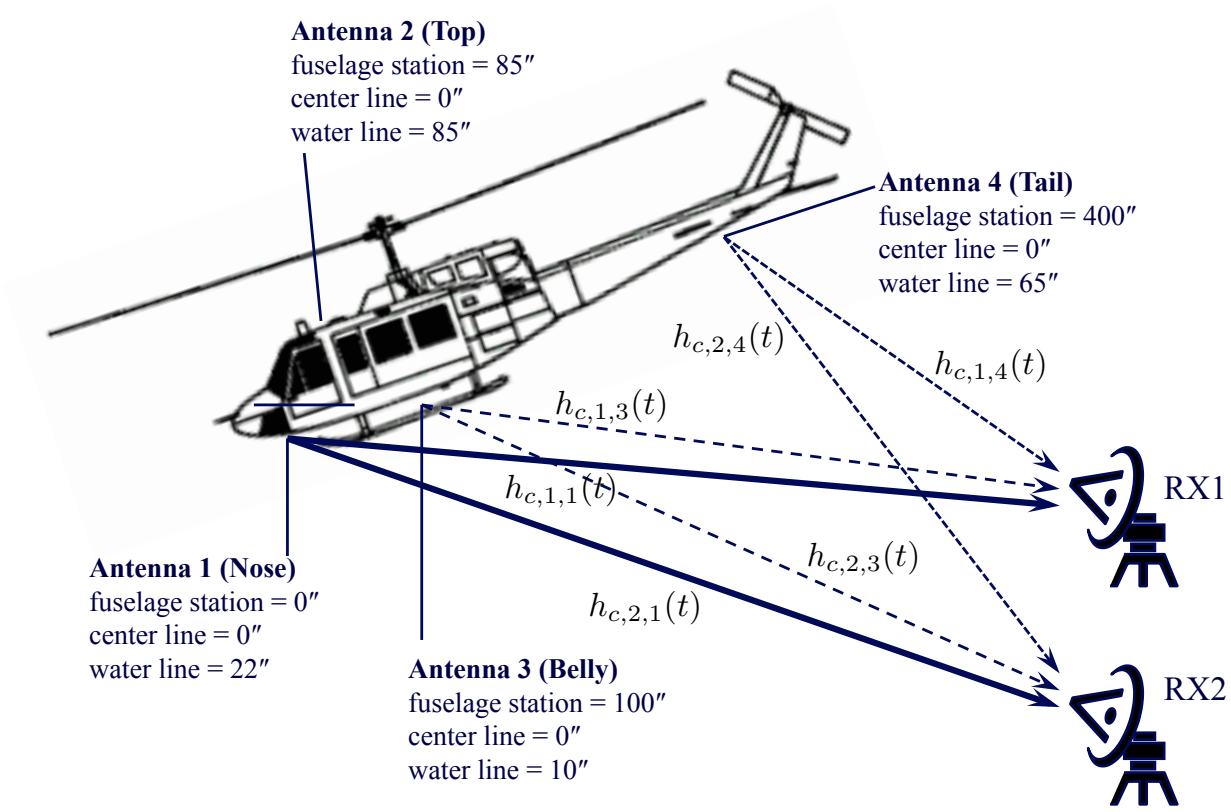

Fig. 8. A diagram of the helicopter-to-ground multi-antenna communications link. Here $h_{c,j,i}(t)$ is the continuous-time impulse response of the channel between transmit antenna i and receive antenna j for $i \in \{1, 3, 4\}$ and $j \in \{1, 2\}$.

Fig. 9. The flight path for the UH-1H helicopter and the locations of the two receive antennas for the multipath channel sounding experiments at Cairns Army Airfield, Ft. Rucker, Alabama. The 2 receive antennas were located on towers at the bottom of the figure.

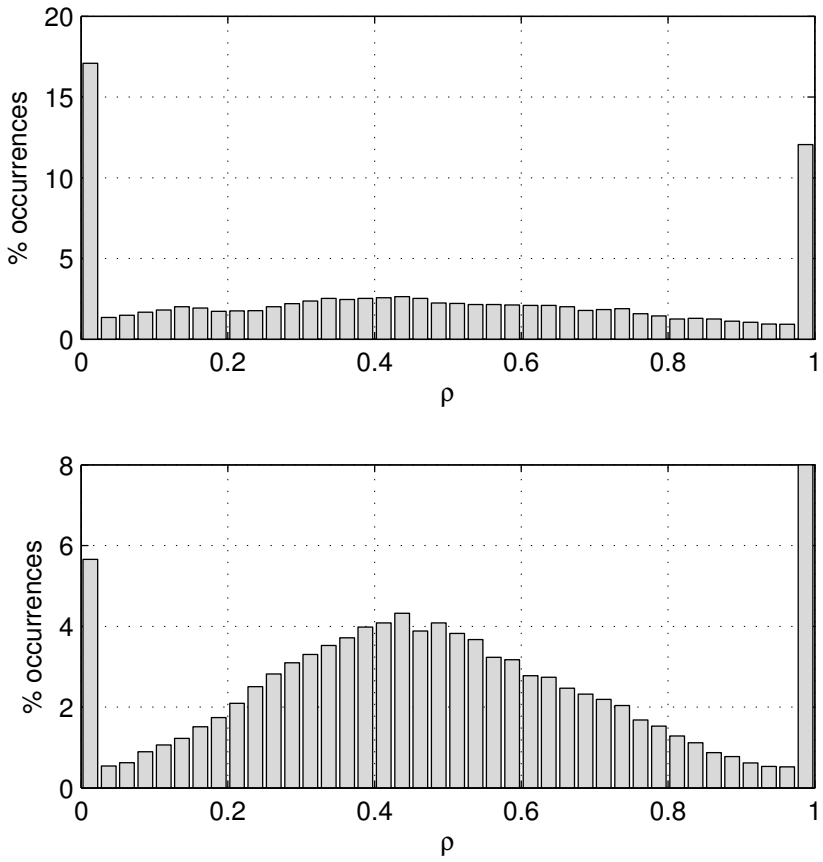

Fig. 10. Optimum power allocations in the mean-squared error sense for the measured channel impulse responses from Cairns Army Airfield, Ft. Rucker, Alabama, using the natural normalization: (top) $E_b/N_0 = 10$ dB; (bottom) $E_b/N_0 = 20$ dB.

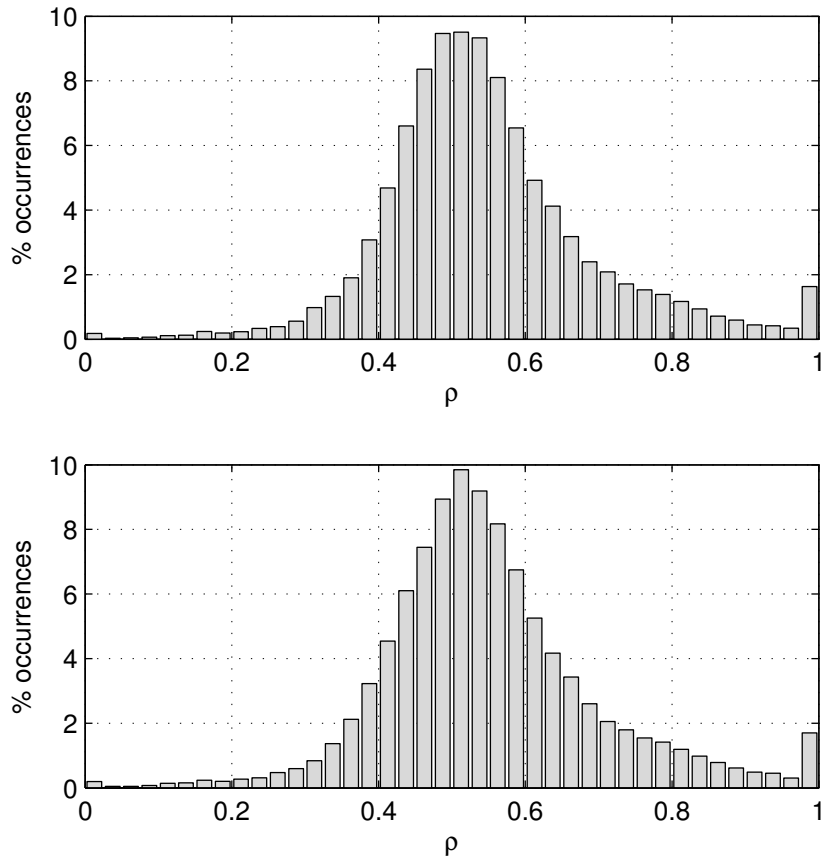

Fig. 11. Optimum power allocations in the mean-squared error sense for the measured channel impulse responses from Cairns Army Airfield, Ft. Rucker, Alabama, using the equal-energy normalization: (top) $E_b/N_0 = 10$ dB; (bottom) $E_b/N_0 = 20$ dB.

B. Edwards Air Force Base, California – Takeoff and Landing

This data set comprises channel impulse responses collected at Edwards Air Force Base, California. Here the transmitter was a Beechcraft C-12 equipped with two transmit antennas as illustrated in Figure 12. The antennas are separated by 79.25 inches (approximately 12 wavelengths at 1824.5 MHz) in the forward/aft direction and 69.5 inches (approximately 11 wavelengths at 1824.5 MHz) in the up/down direction. The ground station, equipped with an 5-meter parabolic reflector autotracking antenna, was located at Building 4795 ($34^\circ\ 58'\ 14.52''$ N, $117^\circ\ 55'\ 52.68''$ W) as shown in Figure 13. The channel sounding signal, occupying 50 MHz of bandwidth and centered at 1824.5 MHz (upper L-band) was used to probe the channel. The resulting impulse responses were resampled to 20 Msamples/s to produce a discrete-time channel for 10 Mbit/s SOQPSK-TG sampled at 2 samples/bit. See [20] for more details.

The focus of this section is the take-off and landing test points on runway 22L as shown in the Figure 13. Building 5790 is approximately 8.75 km from each end of runway 22L and 120 m higher in elevation. This permits a least a partially unobstructed view of the aircraft when it is on either end of the runway. The multipath environment comprises ground reflections and reflections off structures in the line-of-sight path between the aircraft and the ground station tracking antenna. Given the narrow beamwidth of the tracking antenna (approximately 2.3° null-to-null), multipath interference tends to disappear once the aircraft achieves a modest altitude (approximately 175 m above the runway).

To illustrate the behavior of ρ is for take-off and landing, $h_1(n)$ is assigned to the resampled version of the upper-antenna-to-ground propagation path and $h_2(n)$ to the resampled version of the lower-antenna-to-ground propagation path. The geometry is such that the propagation path between the lower antenna and the receiver is partially obscured by the aircraft fuselage. Consequently, $h_1(n)$ is accompanied by a higher signal-to-noise ratio than $h_2(n)$. The lower antenna is further penalized by the presence of a more direct path to the ground-based reflectors that produce multipath. Thus $h_2(n)$ has more ISI than $h_1(n)$. This double penalty of lower signal-to-noise ratio and higher ISI should skew the optimum power allocation in favor of $h_1(n)$ (that is, $\rho \approx 1$).

The results, summarized in Figures 14 and 15 for the 12,564 pairs of channel impulse responses show that this prediction is mostly true. As expected, applying 100% of the available power to the upper antenna dominates the solutions that minimize the mean squared error for both normalization modes: 11,800 or 94% for $E_b/N_0 = 10$ dB and 11,894 or 95% for $E_b/N_0 = 20$ dB with the natural normalization; 11,850 or 94% for $E_b/N_0 = 10$ dB and 11,894 or 95% for $E_b/N_0 = 20$ dB with the equal-energy normalization. The few alternatives to this solution are those where 100% of the available power is allocated to the lower antenna. This is probably

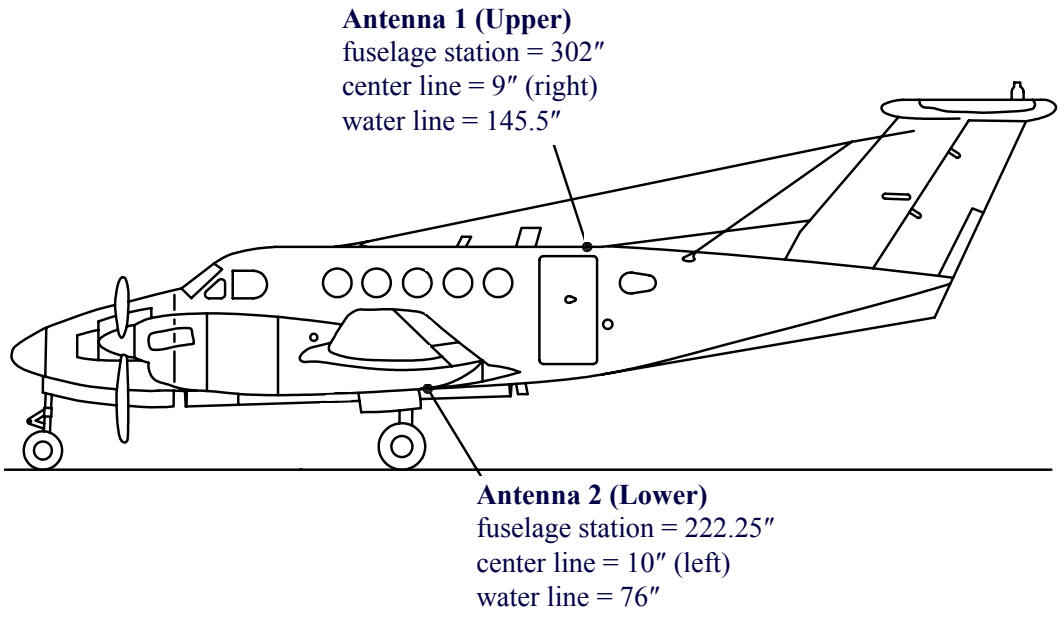

Fig. 12. A diagram of the airborne platform for the channel sounding experiments at Edwards AFB, California, showing the locations of the transmit antennas.

explained by the relatively large spatial separation between the two transmit antennas: when $h_1(n)$ is experiencing significant ISI, $h_2(n)$ can be relatively ISI-free. What's more, when the energy of $h_2(n)$ is significantly below that of $h_1(n)$, the contribution of the ISI associated with $h_2(n)$ to the overall mean squared error is less. The figures show that as signal-to-noise ratio increases, the scenarios where $\rho = 0$ minimizes mean squared error become less frequent.

In summary, the take-off and landing scenario at Edwards AFB, California, is characterized by a geometric arrangement where one of the two channels is inferior in both signal-to-noise ratio and ISI. The solution that minimizes the mean squared error is the one where all the available power is applied to the good antenna, and the percentage of the cases where this is the solution increases with signal-to-noise ratio.

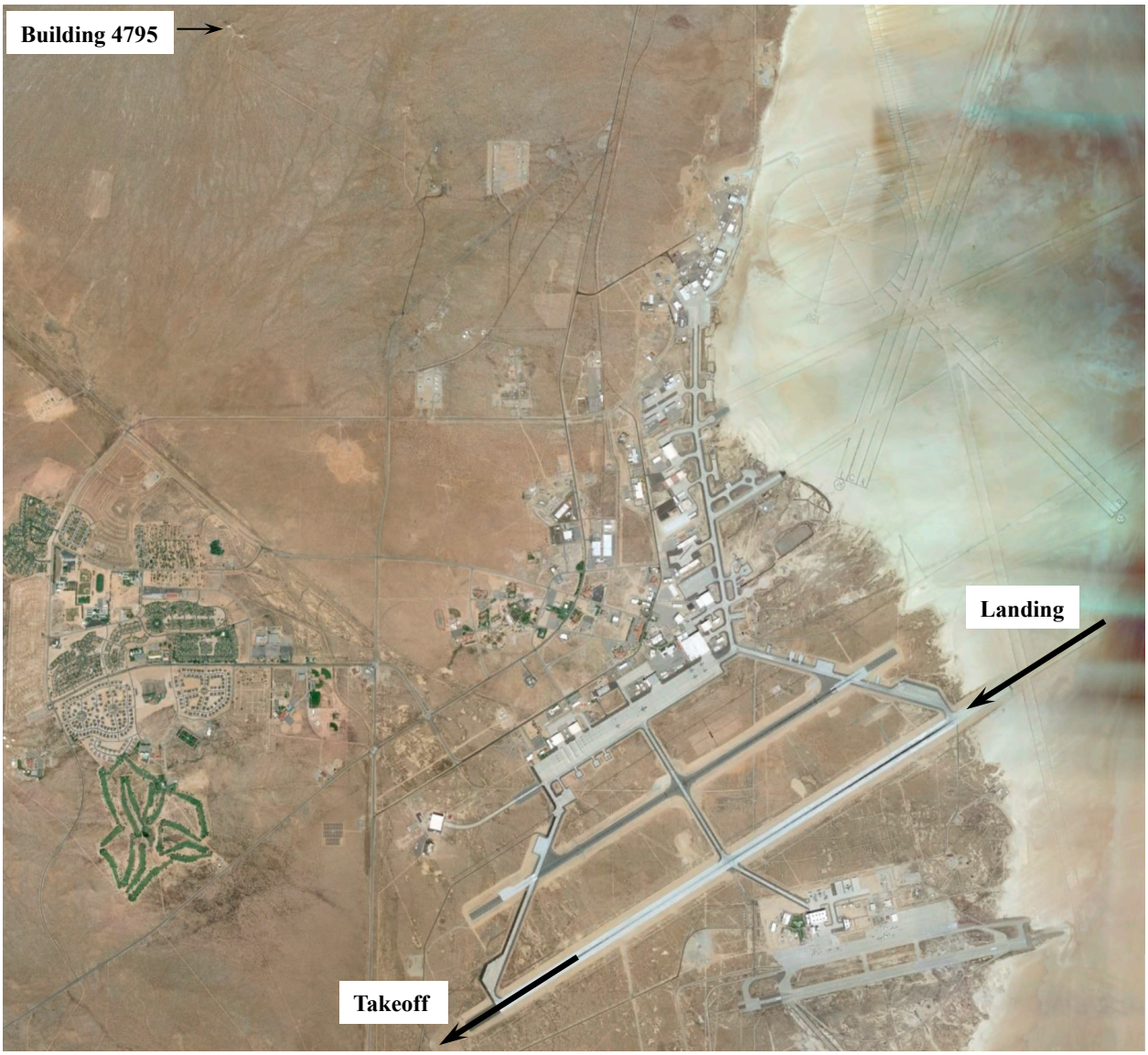

Fig. 13. Map of Edwards AFB, California, showing the location of the ground (receiving) station at Building 4795 (upper left corner of the map) and the locations of the aircraft during take-off and landing (bottom right corner of the map).

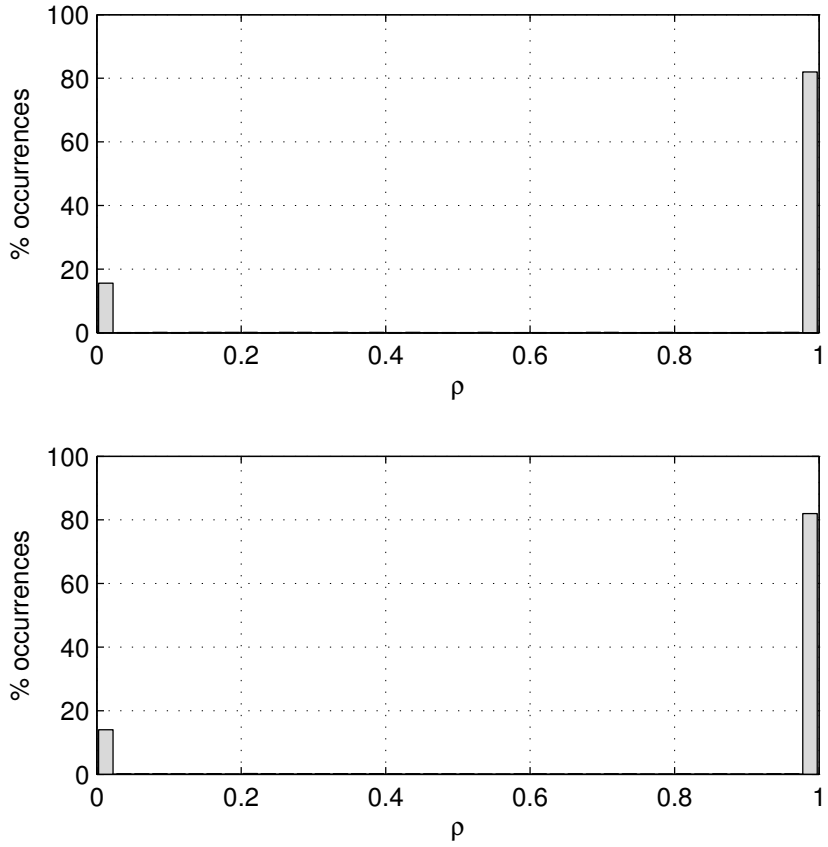

Fig. 14. Optimum power allocations in the mean-squared error sense for the measured channel impulse responses from take-off and landing on runway 22L at Edwards AFB, California, using the natural normalization: (top) $E_b/N_0 = 10$ dB; (bottom) $E_b/N_0 = 20$ dB.

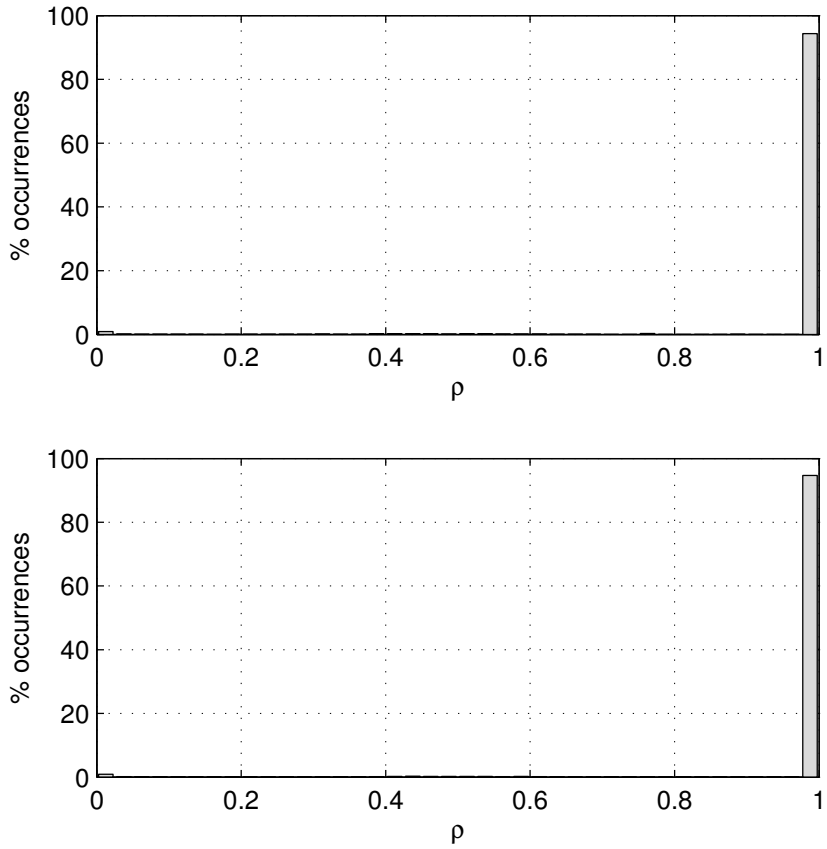

Fig. 15. Optimum power allocations in the mean-squared error sense for the measured channel impulse responses from take-off and landing on runway 22L at Edwards AFB, California, using the equal-energy normalization: (top) $E_b/N_0 = 10$ dB; (bottom) $E_b/N_0 = 20$ dB.

C. Edwards Air Force Base, California – Black Mountain and Cords Road

These two data sets comprise channel impulse responses also collected at Edwards Air Force, California. The airborne transmitter, ground station, and center frequency described in Section V-B were used to obtain these data sets. What is different is the flight path. The two flight paths, called Black Mountain and Cords Road, together with their geographic relationship to the ground station (Building 4795) are shown in Figure 16. The Black Mountain flight path is an east-west flight corridor from $35^\circ\ 12'\ 00''$ N, $116^\circ\ 50'\ 00'$ W to $35^\circ\ 12'\ 00''$ N, $117^\circ\ 56'\ 00'$ W. The Cords Road flight path is also an east-west flight corridor south of the Black Mountain flight path and extends from $35^\circ\ 05'\ 00''$ N, $116^\circ\ 42'\ 00'$ W to $35^\circ\ 05'\ 00''$ N, $118^\circ\ 22'\ 00'$ W. For both flight paths, the airborne transmitter maintained an altitude of $5,000$ feet AMSL. These flight paths are important in that they capture the behavior of low elevation angle "up and away" flight paths. An important characteristic of this flight geometry is the low elevation angle of the receive antenna. The elevation angle is low due to the large distances between the airborne transmitter and the ground based receiver. (Building 4795 is approximately 32 km and 100 km from the west and east ends of the Black Mountain flight path, respectively; 29 km and 111 km from the west and east ends of the Cords Road flight path, respectively.) Because of the low elevation angles, air-to-ground propagation is prone to multipath interference from strong "ground bounces" [21].

As in Section V-B, $h_1(n)$ represents the resampled version of the upper-antenna-to-ground propagation path whereas $h_2(n)$ represents the resampled version of the lower-antenna-to-ground propagation path. Because of the geometry, the upper antenna is partially masked by the aircraft fuselage. Consequently, the signal received from the lower antenna is stronger. Thus $h_2(n)$ is characterized by a higher signal-to-noise ratio than $h_1(n)$. But the lower antenna also illuminates the ground (the source of most of the multipath reflections) with a stronger signal than the upper antenna. Thus although $h_2(n)$ has a higher signal-to-noise ratio than $h_1(n)$, $h_2(n)$ also has more ISI than $h_1(n)$. In this way, the Black Mountain and Cords Road flight paths present a scenario involving a signal-to-noise ratio and ISI tradeoff. How this tradeoff interacts with ρ to minimize the achievable mean-squared error is the open question here.

The results for the 190,716 pairs of channel impulse responses for the Black Mountain flight path are summarized by the histograms in Figures 17 and 18. The results corresponding to the natural normalization are shown in Figure 17. Here, the ISI is such that the equalizer is able to reduce the residual ISI to the point where signal-to-noise ratio is the dominant factor. The end result is that the ISI, signal-to-noise ratio, and power allocation tradeoff becomes mostly a tradeoff between signal-to-noise ratio and power allocation. This tradeoff is such that the mean squared error is minimized by applying 100% of the available power to the lower antenna

[corresponding to $h_2(n)$] in the vast majority of the cases (152,246 or 80% for $E_b/N_0 = 10$ dB, 130,989 or 69% for $E_b/N_0 = 20$ dB). With the equal-energy normalization, the signal-to-noise ratio penalty associated with $h_1(n)$ is removed and the tradeoff reduces to an ISI, signal-to-noise ratio tradeoff. In this case, summarized in Figure 18, the situation reverses. The mean squared error is minimized by applying 100% of the available power to the upper antenna in the vast majority of the cases (147,738 or 77% for $E_b/N_0 = 10$ dB, 155,786 or 82% for $E_b/N_0 = 20$ dB).

The results for the 154,305 pairs of channel impulse responses for the Cords Road flight path are summarized by the histograms in Figures 19 and 20. As expected, the results are similar to those from the Black Mountain flight path. For the natural normalization (Figure 19), the mean squared error is minimized in the majority of the cases, by applying all of the available power to the lower antenna (99,884 or 65% for $E_b/N_0 = 10$ dB, 92,566 or 60% for $E_b/N_0 = 20$ dB). What is different here is that in those cases where this is not true, the preference is to allocate 100% to the upper antenna. This alternate preference becomes less pronounced as signal-to-noise ratio increases. For the equal-energy normalization (Figure 20), the preference reverses and the mean squared error is minimized by applying 100% of the available power to the upper antenna in the vast majority of the cases (116,656 or 76% for $E_b/N_0 = 10$ dB, 124,985 or 81% for $E_b/N_0 = 20$ dB).

In summary, the Black Mountain and Cords Road flight paths are characterized by similar geometries. The channel between the upper antenna and the receiver, $h_1(n)$, is characterized by lower signal-to-noise ratio and lower ISI than $h_2(n)$, the channel between the lower antenna and the receiver. Using the natural normalization, the equalizer is able to remove ISI to the point where signal-to-noise ratio is the dominant factor. In this case applying 100% of the available energy to the lower antenna is the optimum approach in most of the cases. Using the equal-energy normalization, differences in signal-to-noise ratio are removed so that ISI becomes the dominant factor. Because the ISI on the channel from the upper antenna is so much less than the ISI from the lower antenna, applying 100% of the available energy to the upper antenna is the optimum.

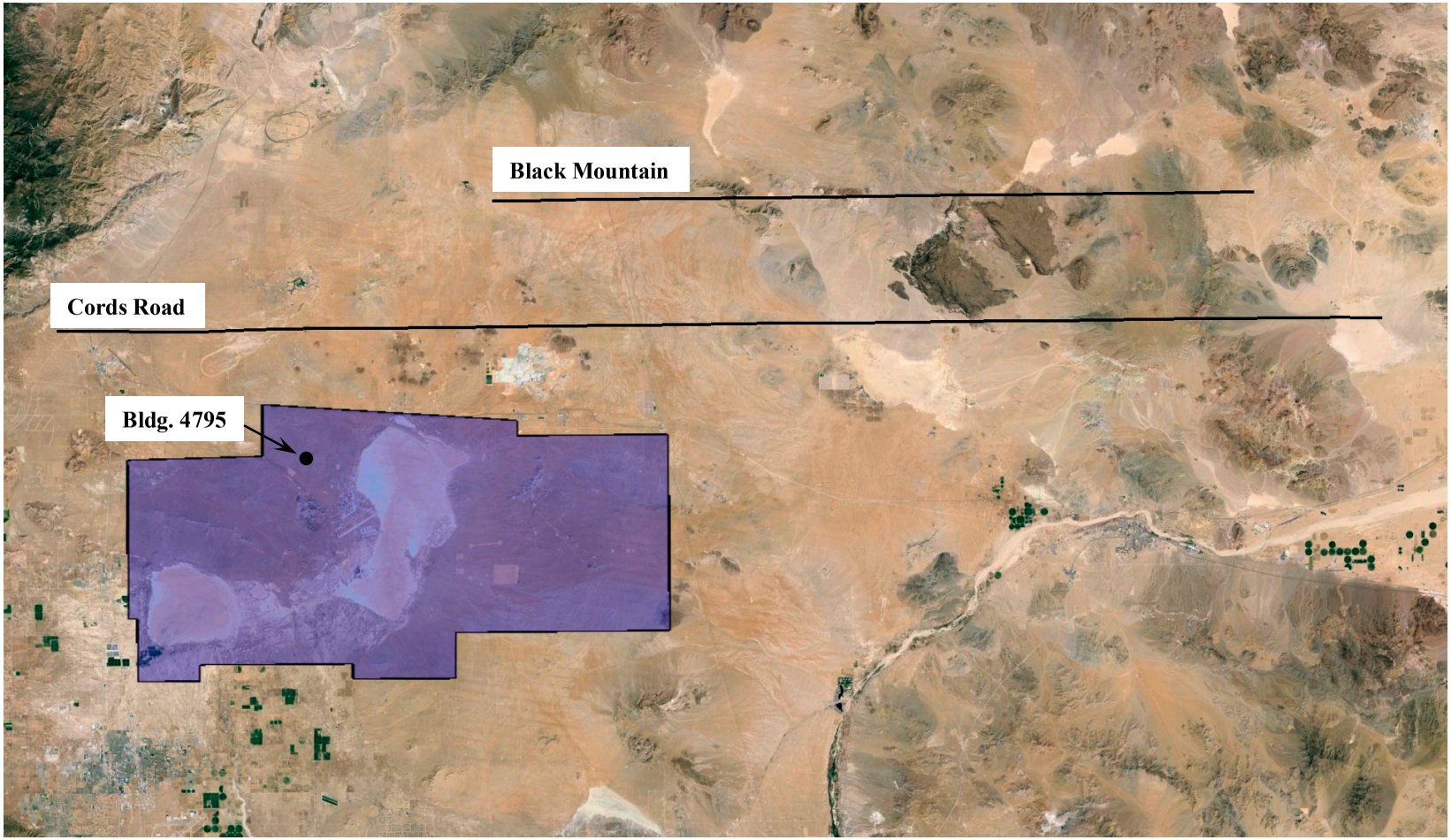

Fig. 16. Map of Edwards AFB, California, showing the location of the ground (receiving) station at Building 4795 and the flight paths for the Black Mountain and Cords Road flight paths.

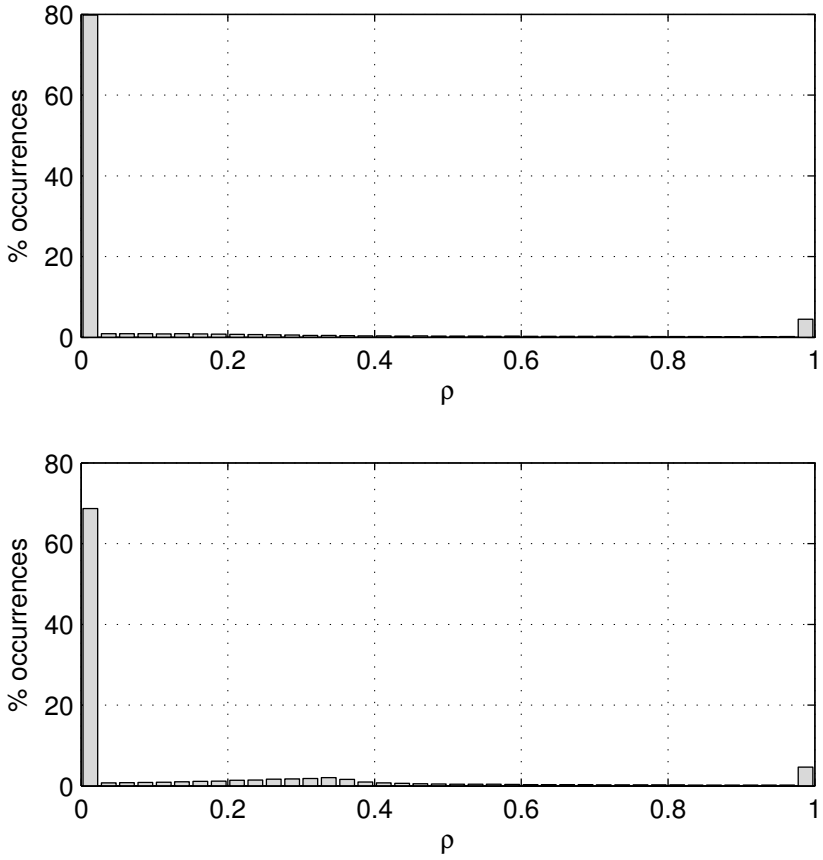

Fig. 17. Optimum power allocations in the mean-squared error sense for the measured channel impulse responses from the Black Mountain flight path at Edwards AFB, California, using the natural normalization: (top) $E_b/N_0 = 10$ dB; (bottom) $E_b/N_0 = 20$ dB.

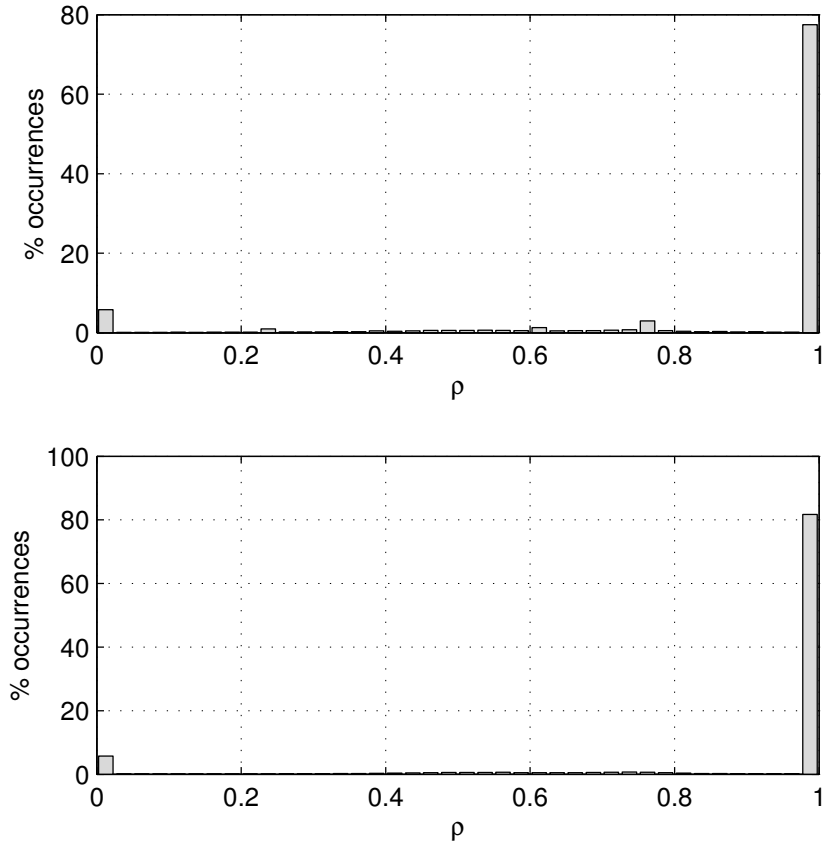

Fig. 18. Optimum power allocations in the mean-squared error sense for the measured channel impulse responses from the Black Mountain flight path at Edwards AFB, California, using the equal-energy normalization: (top) $E_b/N_0 = 10$ dB; (bottom) $E_b/N_0 = 20$ dB.

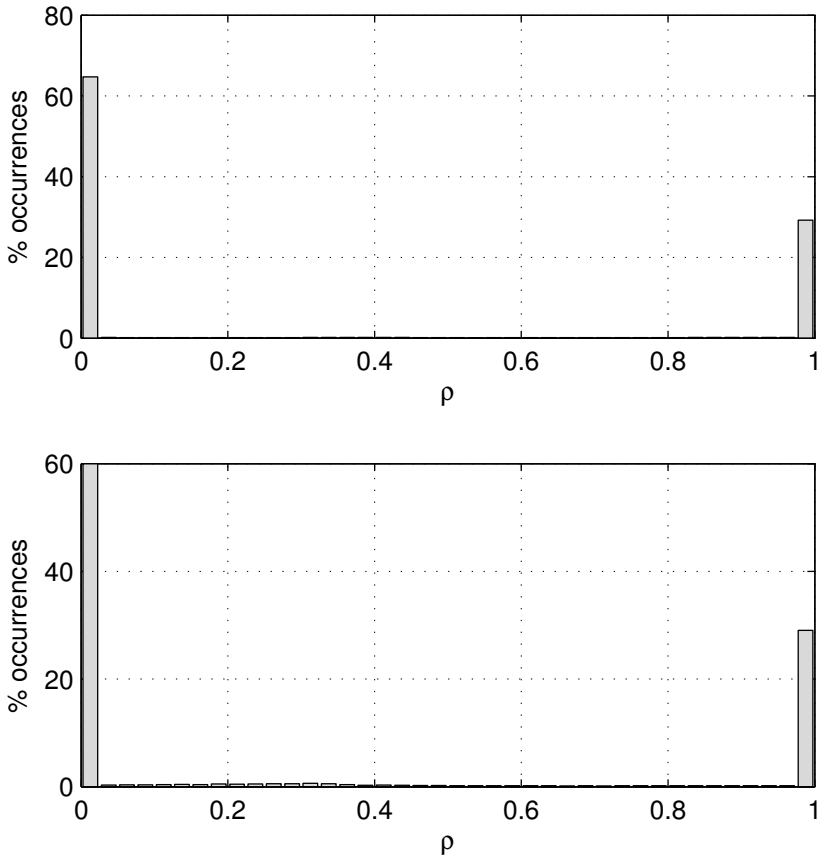

Fig. 19. Optimum power allocations in the mean-squared error sense for the measured channel impulse responses from the Cords Road flight path at Edwards AFB, California, using the natural normalization: (top) $E_b/N_0 = 10$ dB; (bottom) $E_b/N_0 = 20$ dB.

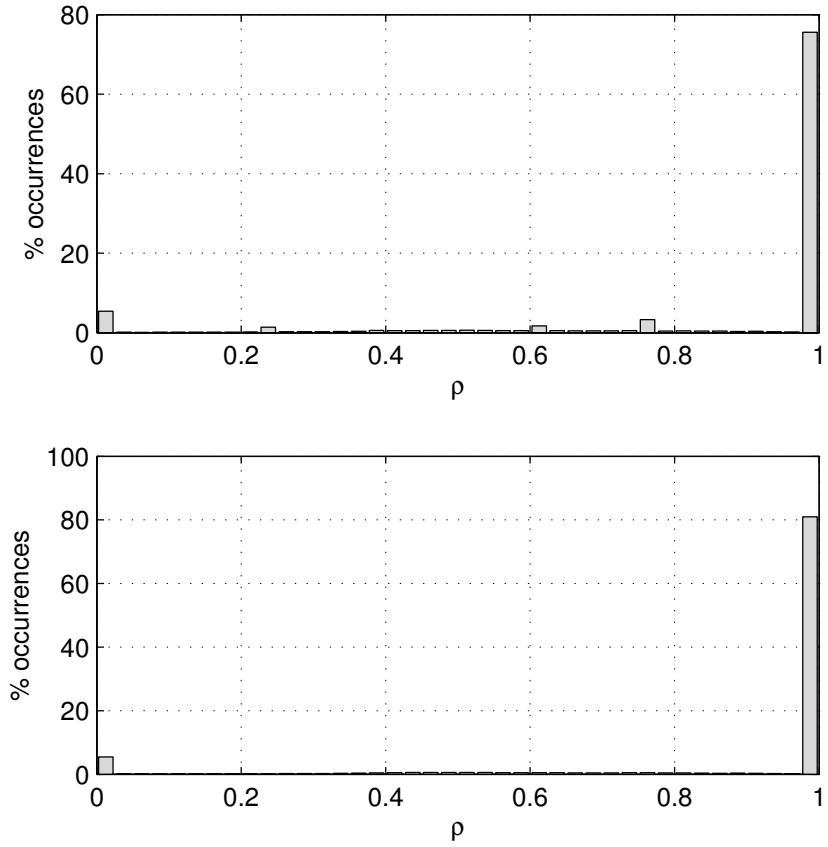

Fig. 20. Optimum power allocations in the mean-squared error sense for the measured channel impulse responses from the Cords Road flight path at Edwards AFB, California, using the equal-energy normalization: (top) $E_b/N_0 = 10$ dB; (bottom) $E_b/N_0 = 20$ dB.

D. A Statistical Model for Triply-Selective Channels

It is interesting to compare these results with what might be inferred from using a simple statistical channel model. To do so, we use a simple Gaussian model for each channel such as that used in [22]. In this experiment, channel 1 comprises 11 IID zero-mean complex-valued Gaussian random variables and channel 2 comprises 18 IID zero-mean complex-valued Gaussian random variables. These numbers, 11 and 18, are the average lengths of $h_1(n)$ and $h_2(n)$, respectively, in the Cairns Army Airfield data set examined in Section V-A. The channels were normalized using the equal-energy normalization described above and 39,300 independent realizations were produced. The results are summarized by the histograms in Fig. 21. The temptation is to think of the optimum ρ as a normally distributed random variable, but it should be kept in mind that this is not the case because $0 \leq \rho \leq 1$. For modest values of E_b/N_0 we observe that the mean value of the optimum ρ is about 0.5. Given the fact that $\rho = 0.5$ corresponds to traditional TR-STBC, we see that the simple statistical model suggests that traditional TR-STBC is the best on average. This is in contrast to the conclusion drawn from the measured channel data, where a strong preference for transmit selection diversity is observed.

As E_b/N_0 increases, the optimum the optimum value of ρ appear to increase. This is explained as follows: as E_b/N_0 increases, the contribution to squared error from additive noise is reduced and ISI starts to become the dominant contributor. The optimum $\rho > 0.5$ means the system prefers to allocate more energy to channel 1 than channel 2. This makes sense because channel 1 is shorter, and this tends to contribute less residual ISI at the equalizer output.

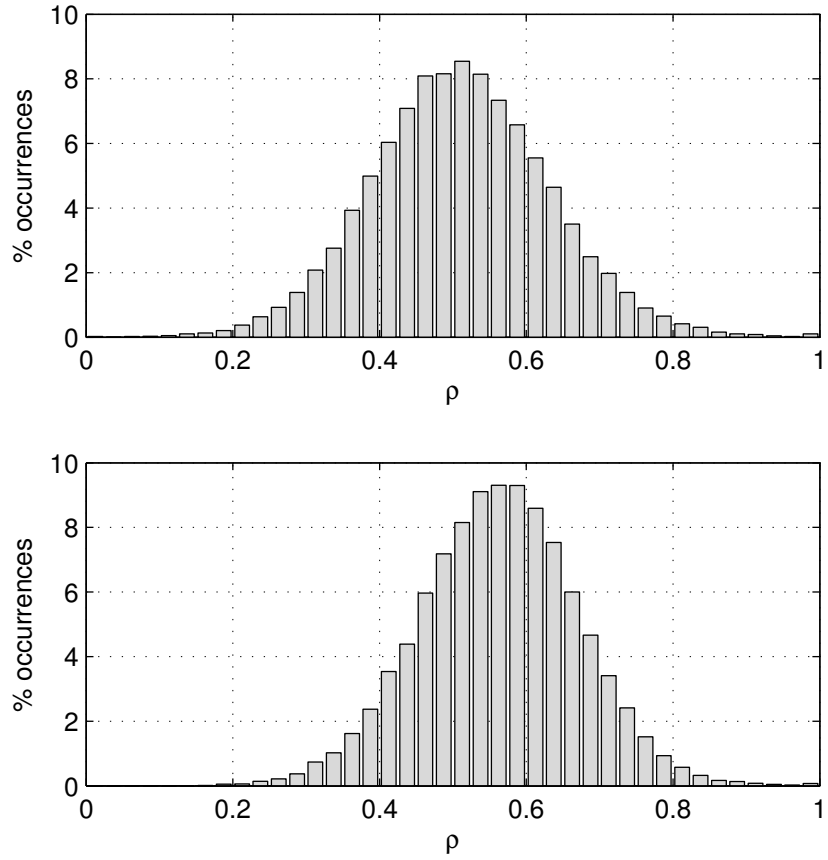

Fig. 21. Optimum power allocations in the mean-squared error sense for pairs of equal-energy channels where the channel coefficients are IID zero-mean complex-valued Gaussian random variables: (top) $E_b/N_0 = 10$ dB; (bottom) $E_b/N_0 = 20$ dB.

VI. Conclusions

A criterion that allows one to predict when it is better to use transmit selection diversity (i.e., one transmit antenna) or the diversity achievable through TR-STBC (i.e., two transmit antennas) was developed. The criterion is the residual mean-squared error at the output of an MMSE equalizer. The residual mean-squared error was not only a mathematically tractable quantity, but also an excellent predictor of the curious behavior illustrated in Fig. 1.

These concepts were applied to a set of measured channel impulse responses collected by sounding experiments in multipath-prone locations at Cairns Army Airfield, Ft. Rucker, Alabama, and Edwards Air Force Base, California. For each pair of channel impulse responses, the value of ρ that minimized the residual mean-squared error (42) was computed. The computed values for ρ were used to form histograms to summarize the results. These results illustrate the following points:

1) In a 2-transmit, 1-receive antenna system operating in a frequency non-selective fading environment, if the two channels have unequal gains, the optimum thing to do is apply all of the available power to the stronger channel. That is, transmit selection diversity is optimum. In contrast, on a frequency selective fading channel, the optimum approach is to apply power to produce the best trade-off between SNR and ISI. That is, transmit selection diversity may not be optimum. The optimum value of ρ associated with the GTR-STBC system described in this paper identifies the best trade-off between SNR and ISI. There are some channel pairs for which $\rho = 0$ or 1 is the optimum (transmit diversity case) and some channel pairs for which $\rho = 1/2$ (traditional TR-STBC). But there are many channel pairs for which neither of these is optimum.
2) On our measured channels, transmit selection diversity was more common than traditional TR-STBC.
3) On a statistical channel, such as the one used in [22], traditional TR-STBC is the best thing to do on average. This is in contrast to the results from the measured channels. Consequently, the optimum power allocation in a real setting is not predicted well by simple statistical channel models.

The expression for the residual mean-squared error (42) was developed by formulating a generalization of TR-STBC that included not only transmit selection diversity and traditional TR-STBC, but also a generalization that permitted the transmitter to allocate unequal power to each transmit antenna. This generalization, called generalized TR-STBC (GTR-STBC), can be used as the basis of transmit diversity system where the transmitter has partial channel state information (in the form of ρ). This transmit diversity system is apropos to single carrier modulations operating in situations with peak-to-average power ratio constraints.

REFERENCES

[1] *IRIG Standard 106-04: Telemetry Standards*, Range Commanders Council Telemetry Group, Range Commanders Council, White Sands Missile Range, New Mexico, 2004, (Available on-line at http://www.wsmr.army.mil/RCCsite/Pages/Publications.aspx).

[2] D. Tse and P. Viswanath, *Fundamentals of Wireless Communication*. Cambridge, UK: Cambridge University Press, 2005.

[3] G. Raleigh and J. Cioffi, "Spatio-temporal coding for wireless communications," *IEEE Transactions on Communications*, vol. 46, no. 3, pp. 357–366, March 1998.

[4] S. Alamouti, "A simple transmit diversity technique for wireless communications," *IEEE Journal on Selected Areas in Communications*, vol. 16, no. 8, pp. 1451–1458, October 1998.

[5] E. Lindskog and A. Paulraj, "A transmit diversity scheme for channels with intersymbol interference," in *Proceedings of the IEEE International Conference on Communications*, New Orleans, June 2000.

[6] N. Al-Dhahir, A. Naguib, and R. Calderbank, "Finite-length MIMO decision feedback equalization for space-time block-coded signals over multipath-fading channels," *IEEE Transactions on Vehicular Technology*, vol. 50, no. 4, pp. 1176–1182, July 2001.

[7] S. Diggavi, N. Al-Dhahir, and R. Calderbank, "Algebraic properties of spacetime block codes in intersymbol interference multiple-access channels," *IEEE Transactions on Information Theory*, vol. 49, no. 10, pp. 2403–2414, October 2003.

[8] W. Gerstacker, F. Obernosterer, R. Schober, A. Lehmann, and L. Lampe, "Equalization concepts for Alamouti's space-time block code," *IEEE Transactions on Communications*, vol. 52, pp. 1178–1190, July 2004.

[9] Y. Zhu and K. Letaief, "Single-carrier frequency-domain equalization with decision-feedback processing for time-reversal space-time block-coded systems," *IEEE Transactions on Communications*, vol. 53, no. 7, pp. 1127–1131, July 2005.

[10] M. Rice and M. Jensen, "Mulitpath propagation for helicopter-to-ground MIMO links," in *Proceedings of the IEEE Military Communications Conference*, Baltimore, MD, October 2011.

[11] M. Rice and M. Saquib, "MIMO equalization for helicopter-to-ground communications," in *Proceedings of the IEEE Military Communications Conference*, Baltimore, MD, October 2011.

[12] J. Proakis and M. Salehi, *Digital Communications*, 5th ed. New York: McGraw-Hill, 2007.

[13] L. Li and M. K. Simon, "Performance of coded OQPSK and MIL-STD SOQPSK with iterative decoding," *IEEE Transactions on Communications*, vol. 52, pp. 1890–1900, November 2004.

[14] T. J. Hill, "A nonproprietary, constant envelope, variant of shaped offset QPSK (SOQPSK) for improved spectral containment and detection efficiency," in *Proceedings of the IEEE Military Communications Conference*, vol. 1, Los Angeles, CA, October 2000, pp. 347–352.

[15] E. Perrins and M. Rice, "Reduced-complexity approach to iterative detection of coded SOQPSK," *IEEE Transactions on Communications*, vol. 55, pp. 1354–1362, July 2007.

[16] T. Nelson, E. Perrins, and M. Rice, "Near optimal common detection techniques for shaped offset QPSK and Feher's QPSK," *IEEE Transactions on Communications*, vol. 56, pp. 724–735, May 2008.

[17] J. B. Anderson, T. Aulin, and C.-E. Sundberg, *Digital Phase Modulation*. New York: Plenum Press, 1986.

[18] E. Perrins, "FEC systems for aeronautical telemetry," *IEEE Transactions on Aerospace and Electronic Systems*, vol. 49, no. 4, pp. 2340–2352, October 2013.

[19] J. Treichler, I. Fijalkow, and C. Johnson, "Fractionally spaced equalizers: How long should they be?" *IEEE Signal Processing Magazine*, May 1996.

[20] M. Rice and M. Jensen, "A comparison of L-band and C-band multipath propagation at Edwards AFB," in *Proceedings of the International Telemetering Conference*, Las Vegas, NV, October 2011.

[21] M. Rice, A. Davis, and C. Bettweiser, "A wideband channel model for aeronautical telemetry," *IEEE Transactions on Aerospace & Electronic Systems*, pp. 57–69, January 2004.

[22] Z. Zhang, T. Duman, and E. Kurtas, "Achievable information rates and coding for MIMO systems over ISI channels and frequency-selective fading channels," *IEEE Transactions on Communications*, vol. 52, no. 10, pp. 1698–1710, October 2004.